



Faculty of Bioscience Engineering

Academic year 2014-2015

Transient coexistence in non-deterministic cyclic species competition

Tim Depraetere

Promotors: Prof. Dr. Bernard De Baets

Dr. Ir. Jan Baetens

Tutor: MSc. Aisling Daly

Master thesis submitted in fulfilment of the requirements for the degree of Master
of Science in Bioscience Engineering: Chemistry and Bioprocess Technology

The author and promoter give the permission to use this thesis for consultation and to copy parts of it for personal use. Every other use is subject to the copyright laws, more specifically the source must be extensively specified when using results from this thesis.

Ghent, June 2015

The promoters,

Prof. Dr. Bernard De Baets

Dr. Ir. Jan Baetens

The tutor,

The author,

MSc. Aisling Daly

Tim Depraetere

Preface

This was by far the most interesting year spend at the Faculty of Bioscience Engineering. For that, I have to thank Dr. Ir. Jan Baetens, MSc. Aisling Daly and Prof. Dr. Bernard De Baets. They provided me with a subject rich in possibilities, and made sure I was free to investigate the options that lie in my field of interest. It is partly because of this that I am now again as fascinated by science as I was during my childhood. Also, they were always able to find time for correcting the text, for providing suggestions or for thinking about solutions to problems.

Tim Depraetere
Ghent, 4 June 2015

Contents

Preface	i
Contents	iv
Summary	v
Dutch summary	vii
1 Background	1
1.1 Modelling microbial communities	1
1.2 Competition	2
1.2.1 Non-transitive competition	2
1.2.2 Cyclic competition	4
1.3 Bacterial interactions	4
1.4 Models for cyclic competition	5
1.4.1 Mean-field equations	5
1.4.2 Partial differential equations	7
1.4.3 Individual-based modelling	8
1.5 Pattern formation	10
2 Non-deterministic cyclic competition: a computational approach	13
2.1 Extensions of the original model	13
2.1.1 Number of species	13
2.1.2 Spatial heterogeneity	14
2.2 Non-deterministic cyclic competition	15
2.2.1 Motivation	15
2.2.2 Simulating non-deterministic competition	15
2.3 Simulation results	18
2.3.1 The parameter space	18
2.3.2 Mobility	24

2.3.3	Number of generations until one species survives	25
2.4	Discussion	26
2.4.1	Bifurcations	26
2.4.2	Survival of the weakest?	26
3	Towards an analytical description of in silico microbial dynamics	29
3.1	Every possible interaction	29
3.2	Coupled map lattice	34
3.3	The mean-field equations	35
3.3.1	Deterministic competition	35
3.3.2	Non-deterministic competition	37
3.4	Partial differential equations	45
3.5	Conclusion	46
4	In-depth study of the governing partial differential equations	47
4.1	Three transients	47
4.2	Travelling waves	48
4.2.1	Lotka-Volterra equations for two species	48
4.2.2	Minimal wave speed	51
4.2.3	Exact solutions	53
4.2.4	Approximating the wave speed	54
4.3	Irregular waves	60
4.4	Transient from initial condition	61
4.5	Conclusion	62
5	Conclusions	63
5.1	Conclusions	63
5.2	Limitations	65
5.3	Extensions	65
	Bibliography	67
A	End-state parameter space at critical mobility	73
B	Coefficients in Section 4.2.4	77

Summary

One of the largest enigmas in ecology is why species manage to coexist, and thus why biodiversity exists. Several explanations have been proposed, of which cyclic competition is one. Species governed by this competition scheme outcompete each other much like rock, paper and scissors do in the popular children's game. A large number of scientific studies has investigated this competition scheme, but all of them considered competition as deterministic. Since diversity also exists among individuals of the same species, it is more realistic to consider non-deterministic competition. This means that although one species usually outcompetes another, it is possible that at some point an individual of the weaker species can outcompete an individual of the stronger species. To make this notion concrete, winning probabilities were introduced, which define the probability of an individual of a species outcompeting an individual of another species.

A literature review was conducted in order to become acquainted with the state-of-the-art of the field, and to determine how non-deterministic competition fits in. Afterwards, an individual-based model was formulated which incorporates the winning probabilities. On the basis of simulations, it was concluded that non-deterministic competition has a strong negative impact on coexistence, although sustained coexistence can occur for certain sets of winning probabilities. Other models were considered to arrive at a more precise explanation of this behaviour. The best results were obtained using partial differential equations, which allowed for the characterisation of coexistence by defining three transients, from which the second transient was examined in depth using analytical methods. This analysis showed that pattern formation is an important facilitator for sustained coexistence, and that the destruction of the patterns, due to an unfavourable combination of winning probabilities, can cut short coexistence. Although the second transient gives an indication of why sustained coexistence occurs for certain sets of winning probabilities, it was concluded that both the first and third transient should be examined too.

Dutch summary

Een van de grootste raadsels binnen de ecologie is de vraag waarom soorten erin slagen samen te leven, en bijgevolg waarom er diverse gemeenschappen bestaan. Verschillende verklaringen hiervoor werden opgeworpen, waarvan cyclische competitie er één is. Soorten die in cyclische competitie treden, beconcurreren elkaar zoals blad, steen en schaar dat doen in het welbekende spel op de speelplaats. Verscheidene wetenschappelijke studies hebben cyclische competitie bestudeerd, maar allen namen aan dat deze deterministisch is. Daar er echter eveneens diversiteit bestaat onder individuen van één soort, is het realistischer niet-deterministische competitie te beschouwen. Dit betekent dat hoewel een bepaalde soort gewoonlijk een andere soort weg concurreert, het nu mogelijk wordt dat een individu van de zwakkere soort een individu van de sterkere soort kan weg concurreren. Om dit concept concreet te maken, werden winstkansen geïntroduceerd. Deze stellen niets anders voor dan de probabiliteit waarmee een individu van een soort een individu van een andere soort weg concurreert.

Door middel van een literatuurstudie werd de stand van zaken binnen het veld in kaart gebracht, en onderzocht hoe niet-deterministische competitie hier binnen past. Vervolgens werd een individu-gebaseerd model voor het simuleren van niet-deterministische competitie ontworpen. Na dit model gesimuleerd te hebben, werd geconcludeerd dat niet-deterministische competitie een sterk negatieve impact heeft op het samenleven van soorten, hoewel voor sommige scenario's een langdurig samenleven mogelijk is. Andere modellen werden bestudeerd met als doel een meer exacte verklaring te geven voor deze bevindingen. De beste resultaten werden behaald door gebruik te maken van partiële differentiaalvergelijkingen. Deze lieten de identificatie van drie transiënten in de evolutie van de *in silico* dynamiek toe, waarvan de tweede transiënt grondig bestudeerd werd, gebruik makend van analytische methoden. Deze analyse toonde aan dat de vorming van ruimtelijke patronen een belangrijke impact heeft op het samenleven van soorten, en dat het verwoesten van deze patronen, bijvoorbeeld door een ongunstige combinatie van winstkansen, het samenleven zeer moeilijk maakt. Hoewel het bestuderen van de tweede transiënt een indicatie levert van waarom langdurig samenleven mogelijk is voor bepaalde combinaties van winstkansen, werd er vastgesteld dat eveneens de eerste en derde transiënten moeten bestudeerd worden om een compleet beeld te krijgen van hoe soorten erin slagen onder niet-deterministische competitie samen te leven.

CHAPTER 1

Background

1.1 Modelling microbial communities

Micro-organisms have played an important role throughout human existence, providing us with fermented foods, drinks and natural selection through diseases. In the near future, they might become even more important. With waste water volumes getting out of hand, fossil resources slowly depleting and a growing demand for new medicines, the human eye is slowly drawn towards micro-organisms and their sheer potential.

However, we only know a small fraction of what there is to know about micro-organisms. This is partly due to the fact that 99 % of all micro-organisms have never been successfully cultured *in vitro*. Such an obstacle, keeping us from acquiring possibly life-changing knowledge, motivates new approaches. By mathematically modelling the more important traits of some species, we might be able to gain a deeper understanding of them, without necessarily having to cultivate them (Ferrer et al., 2008).

Moreover, since communities of micro-organisms are complex assemblies of large numbers of individuals, results from studying them may be applicable to a broader spectrum of social groups, such as mammals (Sherratt et al., 2000). This is because interactions between individuals lead to various kinds of system-level behaviour, and some system-level patterns of bacteria resemble those found in systems of more complex organisms. These parallels make bacteria excellent material for studying the fundamentals of ecology and evolutionary dynamics, since they are relatively easy to cultivate and manipulate (Meyer-Ortmanns and Thurner, 2011).

By cultivating and modelling micro-organisms, we may one day be able to understand two of the most intriguing concepts in evolution and ecology: cooperation and biodiversity. Cooperation involves several organisms working together on providing a public good, beneficial

for all individuals in the population. The catch is that one should expect the existence of selfish intruders, benefiting from the cooperating species' hard labour without cooperating themselves, which may drive the cooperators to extinction. This reasoning implies that cooperation should not occur in nature. However, Gore et al. (2009) have researched yeast working together hydrolysing sucrose, and devised a model which explains why cooperators live on, despite the presence of selfish intruders.

The biodiversity phenomenon, on the other hand, will be the subject of this thesis. Biodiversity is a key aspect to the proper functioning of an ecosystem, and losing biodiversity can cause a total system collapse, since the loss of one species can trigger a cascade of secondary extinctions (Ebenman and Jonsson, 2005). It has been shown that species manage to coexist, thereby maintaining biodiversity, through the formation of spatial patterns, like spirals (Reichenbach et al., 2006).

1.2 Competition

Modelling systems is popular among population biologists. Population biology studies ecological communities consisting of several different species interacting with each other (Hastings, 1997). These interactions can, for instance, involve the competition for resources, like sheep and rabbits competing for their share of the grass, or the more bloody interaction between predators and their prey.

In order to understand the behaviour of a population's dynamics, mathematicians and biologists have proposed and improved several models. The logistic equation, for instance, introduced by the Belgian mathematician Verhulst in 1838, tries to model the growth of a single species (Verhulst, 1838), while around 1925, the well-known Lotka-Volterra equations were devised, modelling the population dynamics in a predator-prey system (Lotka, 1920).

These models, despite being simple, are very informative and enable the description and prediction of population dynamics of several real ecosystems. In this thesis however, the ecosystems considered involve three species that are governed by a very specific competition scheme, called cyclic competition. We will have to dive into more recent literature to come across the more complex models required to aptly describe this behaviour.

1.2.1 Non-transitive competition

As mentioned, an important aim of ecology is to unravel mechanisms which maintain biodiversity and coexistence. As the previous section suggest, modelling population dynamics can be an essential tool to establish whether a group of organisms manages to coexist.

The form of competition governing an ecosystem determines the possibility of coexistence, and therefore studying all possible competition schemes is the key to establish the conditions leading to coexistence. In hierarchical competition, the species involved can be ranked unambiguously in order of their competitive abilities. Thus, if a species A outcompetes some species B, then species A also outcompetes every species outcompeted by species B, while B outcompetes none of the species that outcompete A (Laird and Schamp, 2008). As the *competitive exclusion principle* states: “complete competitors cannot coexist” (Hardin, 1960). Thus when two species compete for the same resource, the one with the best competitive abilities will eventually dominate. The principle therefore makes coexistence less probable in hierarchically organized ecosystems, and this is exactly what makes non-transitive competition interesting to study.

Non-transitive competition is the opposite of hierarchical competition, in that the species involved cannot be ranked unambiguously in order of their competitive abilities. Therefore, under the right conditions, non-transitive competition can result in coexistence.

Several ways for non-transitive competition to manifest itself in nature have been proposed (Laird and Schamp, 2006), and three of them will be described here. They all involve either interference competition or exploitative competition. Interference competition refers to species competing by directly fighting for scarce resources, while exploitative competition refers to species competing indirectly by consuming scarce resources, so that other species experience a shortage for that resource. Non-transitive competition can manifest itself when under exploitation competition, the species in an ecosystem compete for multiple resources and each species competes best for a different resource, yet is limited by some other resource (Huisman et al., 2001; Huisman and Weissing, 1999). In this way, each species can impede the growth of another species by consuming its limiting resource, while in turn being impeded itself by some third species. A large network of species outcompeting and being outcompeted can then exist, which implies non-transitive competition. Non-transitivity also comes to existence when the species’ ranks of exploitation competitive ability differ from their ranks of interference competitive ability, as in this way networks can exist with species outcompeting other species through exploitation competition, while being outcompeted through interference competition. A third possibility occurs in pure interference competition under certain arrangements of toxicity, susceptibility and resistance (Czárán et al., 2002). An example of such competition will be discussed in Section 1.5.

The fact that competitive non-transitivity promotes coexistence has been shown by Laird and Schamp (2006), amongst others. This study involved up to 25 *in silico* species (species that exist in a computer simulation) and several randomly generated competition schemes between these species were constructed. For each competition scheme, an index representing its non-transitivity was calculated. Subsequently, the interactions between the species were

simulated, in a manner similar to the method explained later in Section 1.4.3, to establish whether the particular competition scheme resulted in coexistence. The conclusion of the study was that the non-transitivity of the competition scheme indeed was positively correlated with the species richness at the end of the simulations.

1.2.2 Cyclic competition

For cyclic competition, the simplest form of non-transitive competition, the competition scheme is similar to that of the children's game rock-paper-scissors. Imagine, for example, three species A, B and C that are engaged in cyclic competition. Then A outcompetes B, B outcompetes C and C outcompetes A, as shown in Figure 1.1. Such relationships emerge in several ecosystems around the planet, and involve plants, algae, lizards, bacteria and other species (Kerr et al., 2002). In this thesis, bacteria will be the subject of our investigation, as motivated in Section 1.1.

Notice that with the competition scheme displayed in Figure 1.1, species A always beats species B. One could also design a scheme in which species A beats species B with a certain probability, but not always. The distinction between these two competition schemes is made by calling the first one *deterministic*, and the second one *non-deterministic*.

Models for cyclic competition have been devised by, amongst others, May and Leonard (1975) and Reichenbach et al. (2006), and will be introduced in Section 1.4. First, it is necessary to understand the individual behaviour of micro-organisms, as the models are built on these foundations.

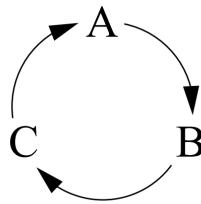


Figure 1.1: Scheme representing cyclic competition between species A, B and C. Species A outcompetes B, B outcompetes C and C outcompetes A.

1.3 Bacterial interactions

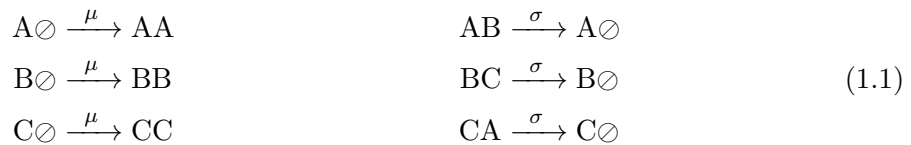
Bacteria are complex beings, and so are their interactions. If a model is to be constructed, simplifications will be necessary. To reduce bacterial interactions to their simplest form, game theory is often relied on (Meyer-Ortmanns and Thurner, 2011). This well-developed branch

of mathematics is concerned with the behaviour of players faced with a certain dilemma: they have to choose between several strategies while playing a simple game.

In the *prisoner's dilemma game* for instance, players may choose to cooperate or to act selfishly. Each scenario is associated with a certain penalty or gain, and so the best strategy for the players can be deduced (Tucker, 1980).

Evolutionary game theory abandons the concept of rational game-play and uses the idea that strategies are inherited programs that control the individual's behaviour. Each species is thus assigned a set of deterministic rules, with which it plays over and over again (Meyer-Ortmanns and Thurner, 2011).

An interaction scheme incorporating cyclic competition was proposed by May and Leonard (1975). Three species, A, B and C, each play by their own set of rules. They all reproduce with rate μ if there is empty space available in their neighbourhood, but each species' game-play is distinguished by the way they undergo selection (with rate σ), as shown in Reactions 1.1. Species A beats B, B beats C and C beats A. From this set of rules, cyclic competition arises. Notice how these reactions can be interpreted as a different representation of the cyclic competition scheme visualised in Figure 1.1.



In the above reactions, \circ represents an empty site, which is not occupied by any bacteria.

1.4 Models for cyclic competition

1.4.1 Mean-field equations

Lotka-Volterra equations

On a microscopic scale, the occurrence of the interactions introduced in Section 1.3 is essentially stochastic, as the underlying molecular processes are often inherently stochastic, and there is variability between the individuals of the species involved (Meyer-Ortmanns and Thurner, 2011). Assuming that the populations are of infinite size, however, these interactions can be modelled through the use of deterministic systems, rather than stochastic ones. The interactions of the individuals are then averaged into a single population-level effect, which usually gives rise to a system of nonlinear ordinary differential equations (ODEs) (Jovanovic

and Rosenthal, 1988). This approach, called the mean-field approximation, originated from physics and was later used in economics and biology (Weiss, 1907).

The Lotka-Volterra equations, modelling the population of predators and prey through time, will be used to illustrate this approach (Lotka, 1920). A number of fish $x(t)$ (prey) and sharks $y(t)$ (predators) populate an ecosystem in the ocean. The fish eat plankton, which is assumed to be abundantly available, and the sharks, when feeling hungry, eat the fish they encounter. The interactions between sharks and fish are subject to variability, which is due to, for instance, the number of encounters between fish and sharks in a certain amount of time, the amount of time since a shark's last meal, and the fitness of a shark or fish due to age or injury. By using the mean-field approximation, one is able to average all these stochastic variables, resulting in one averaged effect.

Since the amount of available plankton is assumed to be infinite, the average per capita growth rate of the fish population in the Lotka-Volterra equation is constant, so that, in absence of sharks, the change of the fish population over time satisfies the ODE $\dot{x} = \lambda x$, where \dot{x} denotes the derivative of x with respect to time. The sharks, on the other hand, in the absence of fish, have nothing to eat, and their population in this scenario would decay according to $\dot{y} = -\mu y$. The presence of fish increases the sharks' per capita growth rate to $-\mu + cx$. Finally, the fish are being eaten, decreasing their per capita growth rate to $\lambda - by$. Combining these growth rates gives rise to the Lotka-Volterra equations:

$$\begin{cases} \dot{x} = x(\lambda - by), \\ \dot{y} = y(-\mu + cx). \end{cases}$$

As such, the stochastic system is replaced by a deterministic system of nonlinear ODEs, with parameters λ , μ , b and c , using the mean-field approximation (Brauer and Castillo-Chávez, 2001).

Mean-field equations for cyclic competition

The same rationale as the one leading to the Lotka-Volterra equations can be used to obtain mean-field equations for the cyclic competition scheme we are interested in, by considering Reactions 1.1. This gives rise to the following system of ODEs (Reichenbach et al., 2008):

$$\begin{cases} \dot{a} = a[\mu(1 - \rho) - \sigma c], \\ \dot{b} = b[\mu(1 - \rho) - \sigma a], \\ \dot{c} = c[\mu(1 - \rho) - \sigma b], \end{cases} \quad (1.2)$$

where μ denotes the reproduction rate, σ the selection rate, a , b and c the densities of species A, B and C, respectively, and ρ the total density ($\rho = a + b + c$).

The evolution of species A's density through time (\dot{a}) increases through reproduction and decreases through selection. The amount of increase is dependent on the reproduction rate, the population of species A and the amount of free space ($1 - \rho$). This term basically represents the probability of a member of species A reproducing in an empty space. The decrease, on the other hand, is dependent on the selection rate and the population sizes of species A and C. The corresponding term represents the probability of a member of species A being killed by a member of species C. Notice that the probability of two species encountering each other, and the probability of any species finding an empty space for reproducing, is only dependent on the population of the species in the whole system, and not on their spatial configuration. Therefore, and because this system of equations was derived using the mean-field approximation, it only holds for a well-mixed system with a large number of individuals, an important and restrictive assumption (Reichenbach et al., 2008).

1.4.2 Partial differential equations

As stated in Section 1.1, the formation of spatial patterns, such as spirals, is a key aspect in maintaining coexistence. Despite being simple and very informative, System ((1.2)) does not involve any spatial degree of freedom, and therefore is not adequate to study coexistence. Moreover, bacteria are mobile beings, and the mean-field equations ignore this important property of bacteria (Reichenbach et al., 2008).

To overcome this shortcoming, the following partial differential equations (PDEs) can be constructed:

$$\begin{cases} \frac{\partial a}{\partial t}(\mathbf{r}, t) = D \Delta a(\mathbf{r}, t) + \mu a(\mathbf{r}, t) [1 - \rho(\mathbf{r}, t)] - \sigma a(\mathbf{r}, t) c(\mathbf{r}, t), \\ \frac{\partial b}{\partial t}(\mathbf{r}, t) = D \Delta b(\mathbf{r}, t) + \mu b(\mathbf{r}, t) [1 - \rho(\mathbf{r}, t)] - \sigma b(\mathbf{r}, t) a(\mathbf{r}, t), \\ \frac{\partial c}{\partial t}(\mathbf{r}, t) = D \Delta c(\mathbf{r}, t) + \mu c(\mathbf{r}, t) [1 - \rho(\mathbf{r}, t)] - \sigma c(\mathbf{r}, t) b(\mathbf{r}, t), \end{cases} \quad (1.3)$$

with $\mathbf{r} = (r_1, \dots, r_d)$ in d -dimensional space, D a diffusion constant and Δ the Laplacian operator. In this way, population densities are now functions of both space and time. In addition, diffusion is introduced, so that bacteria can move through the considered continuous space (Reichenbach et al., 2008).

1.4.3 Individual-based modelling

The models described in the previous subsections are the result of a top-down approach. They use population-averaged values to characterize the individual bacteria, therefore local phenomena and variability among species are neglected. These traits may, however, be the key to understanding the behaviour exhibited by a system of bacteria in cyclic competition. In addition, top-down approaches will not be of much use when examining how a specific property of a bacteria influences the behaviour of the species on a macroscopic level.

Thanks to computers becoming increasingly faster, we can seize the opportunity to apply the game theoretical ideas and concepts introduced in Section 1.3, which describes interactions between individuals, on a massive scale. We can design an *in silico* ecosystem involving numerous members of several species, and subsequently let individuals interact with their neighbours, to then assess how the collective behaves. Each individual can be assigned its own strategy for playing a certain game, thus introducing variability. This bottom-up approach is called individual-based modelling, and makes use of an individual-based model (IBM) (Ferrer et al., 2008).

In our case, three different species populating such an *in silico* ecosystem are assigned the rules expressed by Reactions 1.1, complemented with the possibility of migration. This individual behaviour is then simulated in a two-dimensional space, so that the consequences of the individual sets of rules result in a certain system-level behaviour, also known as emergent behaviour. The microscopic interactions thus give rise to a certain macroscopic strategy for each species.

Individual-based modelling, being a unique way of working, creates several possibilities. One can learn how applying certain rules to individuals influences the overall behaviour of the system. Conversely, one can explore which set of rules mimics the system-level behaviour observed by plating out micro-organisms and examining the system's behaviour through a microscope. An IBM can also be used as an alternative to experimental studies when these, for instance in microbiology, are difficult to perform and expensive in terms of time and cost. A hypothesis can then, up to a certain level, be compared to the results of an IBM, rather than to the outcome of the tedious plating out of micro-organisms (Ferrer et al., 2008).

Individual-based modelling for cyclic competition

An algorithm introduced by Gillespie (1977), originally intended for simulating chemical reactions, can be used to simulate an IBM involving bacteria, in two dimensions.

A square grid is divided in a number of square cells of equal size, for instance 100×100 . Then, each of the cells is filled randomly with either a bacteria of a certain species or is left empty.

Then, at each simulation step, a randomly selected cell interacts with one of the cells in its neighbourhood. Interacting involves either: reproduction, with probability $\mu/(\mu + \sigma + \epsilon)$; selection, with probability $\sigma/(\mu + \sigma + \epsilon)$ or migration, with probability $\epsilon/(\mu + \sigma + \epsilon)$. A neighbourhood in our case is defined as the von Neumann neighbourhood, which comprises the four cells orthogonally surrounding a central cell (Von Neumann and Burks, 1966). In the case of a migration event, a bacteria will swap places with an adjacent bacteria, or with an empty space. This happens at rate ϵ and makes the bacteria mobile. The possible interactions are schematically displayed in Figure 1.2. Species C (blue) kills species B (yellow) during a selection event, and an empty cell remains. When an empty cell is available, an individual in an adjacent cell can reproduce. This is what species A (red) does in this example. At the bottom of the image, species B and species C exchange places in a migration event (Reichenbach et al., 2007).

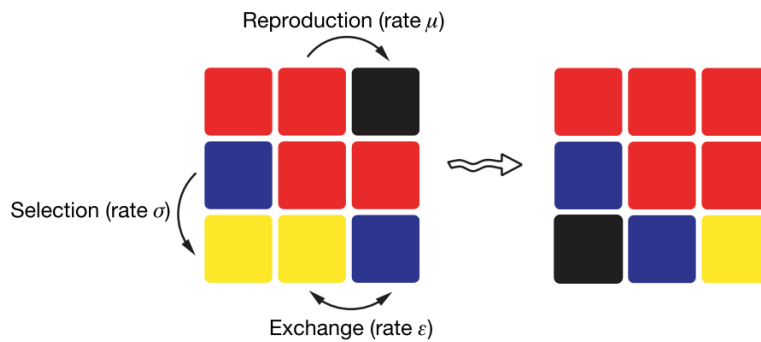


Figure 1.2: Members of three species A (red), B (yellow) and C (blue) occupy squares on a 3×3 grid. Selection (with rate σ), reproduction (with rate μ) and migration (with rate ϵ) are displayed (Reichenbach et al., 2007).

At the end of each simulation step, the outcome of the interaction is calculated, and the grid is updated, meaning that the two cells involved in the interaction are assigned their new state (empty or occupied by a species) accordingly. Figure 1.3 displays the flow-chart followed in every consecutive simulation step.

Figure 1.4 shows an example of the spatio-temporal evolution of an *in silico* microbial community starting from (a) an initially random configuration, after (b) 5, (c) 13, (d) 44, (e) 100 and (f) 200 generations, governed by the model described in Section 1.4.3, on a 250×250 grid. After some generations, due to the cyclic nature of the competition scheme, spiral waves emerge. For low mobilities (low migration rate ϵ), the radius of these spiral waves is small, and coexistence is maintained. However, when mobility reaches a threshold, the spirals grow larger than the size of the system, and eventually only one species remains while the others

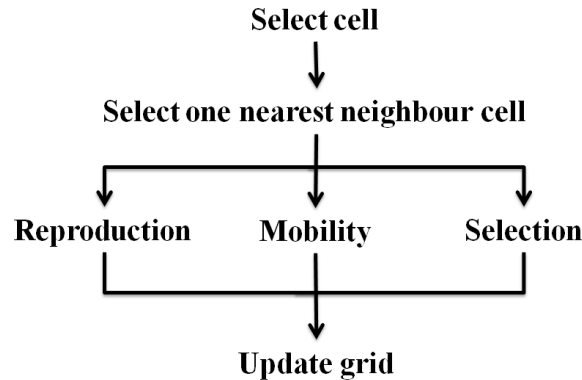


Figure 1.3: Flow-chart followed in each simulation step of the algorithm introduced by Gillespie (1977). A random cell is selected together with one of its four nearest neighbours. Subsequently, the individuals inhabiting the cells undergo a certain interaction, after which the grid is updated.

have died out (Reichenbach et al., 2007). In Figure 1.4, the mobility is low enough to maintain coexistence.

In Section 2.2 we will show how we have modified this foundational model to meet the needs of our specific research.

1.5 Pattern formation

A notable real-life example in which pattern formation is observed is the cyclic competition between three strains of *Escherichia coli*. The set-up of the experiment conducted by Kerr et al. (2002) was the following. An ecosystem consisting of a colicin-producing strain, a colicin-sensitive strain and colicin-resistant strain were cultivated in a flask and a static plate, introducing an environment with high and low mixing, respectively. The nature of the cyclic competition can be understood from the following facts. The colicin-producing strain outcompetes the colicin-sensitive strain by killing it. The colicin-sensitive strain outcompetes the resistant strain by growing faster, as they do not have to produce the necessities for becoming resistant. Finally, the colicin-resistant strain outcompetes the colicin-producing strain, as this last strain needs to be resistant and produce colicin, and therefore grows the slowest. The governing competition scheme is shown in Figure 1.5(a).

In the flask environment, two strains went extinct soon after the experiment had begun. Coexistence thus seemed to be unlikely. On the static plate, however, all three species maintained high densities throughout the experiment. This phenomenon was explained by the spatial pattern formed by the organisms on the static plate, which was hindered in the flask

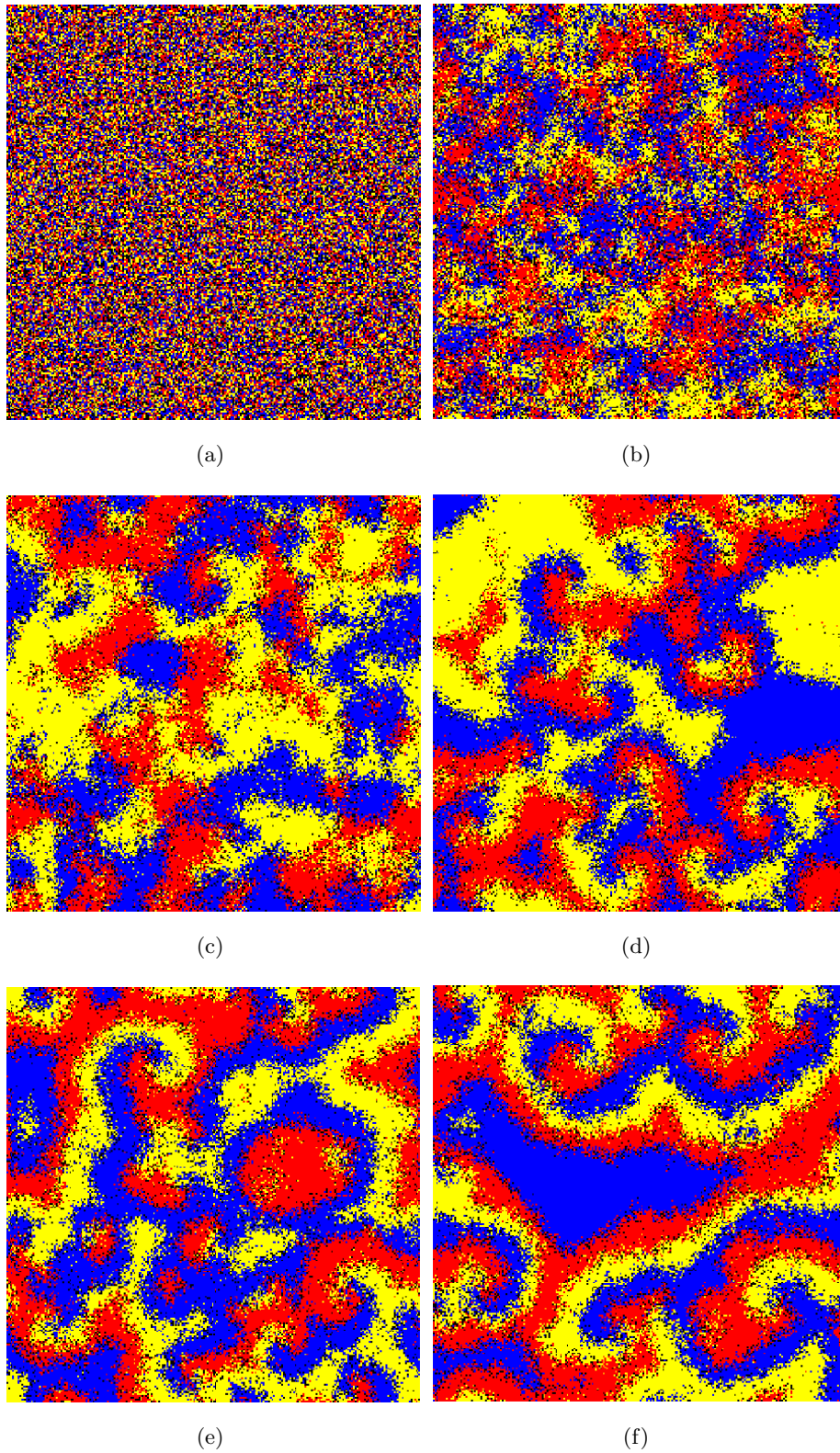


Figure 1.4: These figures show the spatio-temporal evolution of the *in silico* microbial community starting from (a) a random initial configuration, after (b) 5, (c) 13, (d) 44, (e) 100 and (f) 200 generations, governed by the model described in Section 1.4.3. Three species interact according to a cyclic competition scheme, and thus species A (red) invades species B (blue), B invades species C (yellow) and C invades A.

environment due to the constant mixing. The spatial structures are a result of a balanced chase, in which for example the colicin-producing strain invades the colicin-sensitive strain, while being invaded by the colicin-resistant strain, as shown on Figure 1.5(b). This experiment illustrates the shortcomings of the mean-field approach (cfr. Section 1.4.1), as the assumption of well-mixedness makes it impossible to study the essential spatial features an ecosystem governed by cyclic competition exhibits. While indeed locally two species will go extinct, somewhere else on the petri dish this might not be the case, and thus a balanced chase develops and coexistence occurs.

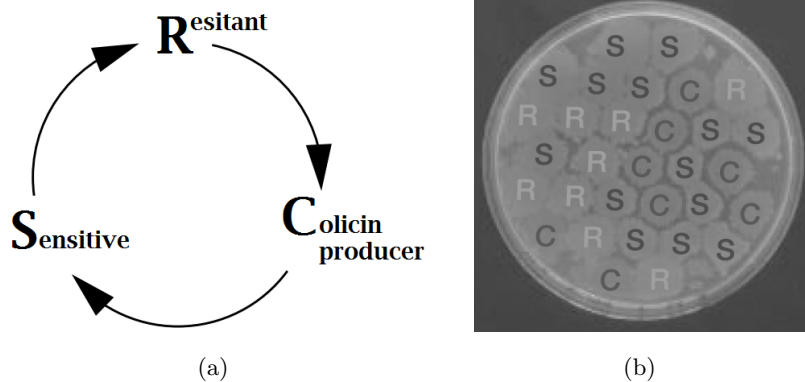


Figure 1.5: The cyclic competition scheme for a colicin-producing strain, a colicin-sensitive strain and a colicin-resistant strain of *Escherichia coli* (a) and the in vitro ecosystem obtained after plating out the species on a static plate (b) Kerr et al. (2002).

Laird (2014) modelled the *Escherichia coli* ecosystem using an IBM similar to the one discussed in Section 1.4.3, finding that the simulation results closely matches the results of the study by Kerr et al. (2002). Laird (2014) highlighted the importance of pattern formation by running simulations with differing spatial interaction structures. While in some simulations, individuals were allowed to interact with their four nearest neighbours, other simulations used a more random spatial interaction structure, in which a varying number of the regular, four nearest neighbour spatial interactions were replaced by interactions with a random cell on the grid.

The simulations showed that interaction with nearest neighbours resulted in coexistence, while only small deviations towards a more random spatial interaction structure prevented strain coexistence. This demonstrates that coexistence is not merely due to the limited number of possible individuals to interact with in two-dimensional space (in this case four), but rather that space itself, and thus the formation of spatial patterns, is essential for coexistence.

CHAPTER 2

Non-deterministic cyclic competition: a computational approach

2.1 Extensions of the original model

Models are an approximation of reality. Since the model proposed by May and Leonard (1975) is quite well understood today, it is now possible to make it more realistic by extending it. In the following subsections, two extensions of the original model are presented. One considers a higher number of species, and the other spatial heterogeneity. Our own adaptation of the original model, which will be the subject of the remainder of this thesis, is introduced in Section 2.2.

2.1.1 Number of species

A minimum of three species is required to construct a non-transitive competition scheme, which makes the rock-paper-scissors model the simplest one for studying this aspect of coexistence. In nature, however, most ecosystems consist of more than just three species, which makes a more complex model involving more diverse communities a logical extension.

Liard and Schamp (2006) performed IBM simulations involving up to 25 species. The conclusion was that the species richness at the end of the simulation was positively correlated with the initial species richness, where species richness is the number of species present in the ecosystem. Moreover, the number of coexistent species was also positively correlated with the non-transitivity of the rather complex competition scheme. Highly non-transitive communities of high species richness should thus be able to coexist.

More extensive research has been conducted for competitions involving four or five species. The competition scheme investigated by Lutz et al. (2013), for instance, is shown in Fig-

ure 2.1(a). It involves four species in cyclic competition and introduces a parameter χ that denotes the rate of interaction beyond the single loop connecting the species. As χ increases from zero to infinity, and thus the rate of interaction beyond the single loop, the competition scheme becomes more hierarchical as species one and two then have two preys each and one predator. The researchers found that four species are able to coexist as long as χ remains lower than a critical value of $\chi_c \simeq 0.355$. Above this value, the system decreases the transitivity of the competition scheme by the extinction of one species, after which the remaining three species coexist.

Cheng et al. (2014) studied five species in cyclic competition and the influence of mobility. They found that in different regions, local communities of three species can coexist. As the composition of these local communities varied, the species richness over the entire space was determined by the interactions between these communities, mediated by mobility. For low mobility, five species managed to coexist. However, upon increasing the migration rate, two transitions occurred: first from five- to three-species coexistence and then from three-species coexistence to a monoculture. These results are similar to the critical mobility observed in the rock-paper-scissors game by Reichenbach et al. (2007).

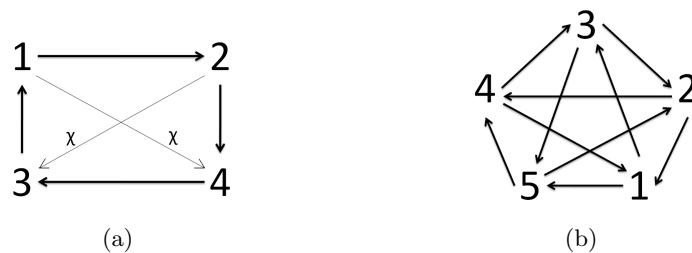


Figure 2.1: Competition schemes involving four species Lutz et al. (2013) (a) and five species Cheng et al. (2014) (b).

2.1.2 Spatial heterogeneity

Typically, all cells in an IBM have the same properties. In reality, however, one can imagine that, for example, the amount of available resources will be distributed unevenly across the space where a community of species resides. The question then arises whether this spatial heterogeneity has an impact on the possibility of coexistence. Allesina and Levine (2011) tried to answer this question by simulating 100 species whose competitive abilities were ranked randomly for five limiting factors. These factors could, for instance, represent resources which the species need in order to grow or compete. The grid inhabited by the species was then divided into patches, and each patch was assigned a certain number of each of the five limiting factors. The 100 species were then allowed to compete on the grid.

In each patch, extinction events occurred until the ecosystem settled down to coexistence of a limited number of species, determined by their competitive abilities regarding the limiting factors and the connectivity of the competition scheme, as one would expect. However, as all patches held different combinations of limiting factors, the types of species that coexisted differed from patch to patch. Subsequently, the total number of different species coexisting over all of the different patches was higher than what would be observed if the resources were distributed in a spatially homogeneous way. Thus coexistence benefits from spatial heterogeneity.

Schreiber and Killingback (2013) conducted a similar study, with the extension that individuals were now allowed to diffuse from patch to patch. They concluded that coexistence can benefit from a sufficient degree of spatial heterogeneity when mobility is low enough.

2.2 Non-deterministic cyclic competition

2.2.1 Motivation

The competition scheme shown in Figure 1.1 is deterministic since species A always beats species B. This is, however, not a realistic assumption, as there is diversity among individuals of the same species. Some member of species B may be more apt to compete with the members of species A than the rest of its peers, and vice versa. An individual may even be more prone to selection dependent on its age or the amount of sunlight it receives at a certain time of day. Therefore, it is more realistic to resort to stochastic competition schemes, which will be the main focus of the remainder of this thesis.

Hence, we introduce winning probabilities P_1 , P_2 and P_3 , ranging between 0 and 1, as shown in Figure 2.2. Species A now beats species B with winning probability P_1 , B beats C with winning probability P_2 and finally C beats A with winning probability P_3 . Moreover, species B can now beat species A with probability $(1 - P_1)$, and so on.

2.2.2 Simulating non-deterministic competition

In order to understand how the non-determinism influences coexistence between three species, computer simulations were conducted using the IBM discussed in Section 1.4.3, with the modification of non-deterministic cyclic competition as explained above. To make communication easier, we define sustained coexistence as three species living together for a significant amount of time, while coexistence is defined as three species living together for any amount of time. These definitions hold for the remainder of the thesis.

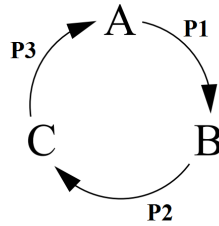


Figure 2.2: Scheme representing non-deterministic cyclic competition between species A, B and C. Species A only beats species B with a winning probability P_1 while B beats A with probability $(1 - P_1)$, and so on.

Through the IBM simulations, one is able to investigate for which combinations of winning probabilities P_1 , P_2 and P_3 , sustained coexistence is likely to occur, and one can attempt to qualitatively describe the conditions necessary for sustained coexistence.

Experimental set-up

The algorithm used to simulate the interactions between the bacteria has been outlined in Section 1.4.3. In order to avoid boundary effects, periodic boundary conditions were imposed, so that the grid may be envisaged as a torus. The bacteria were allowed to interact for 10 000 generations on a 100×100 grid. *In silico*, a generation is defined such that, on average, every cell has been randomly selected once. On a 100×100 grid, this means that 10 000 interactions constitute a generation, or equivalently, that the algorithm has to run 10 000 times through the flow-chart in Figure 1.3.

Experiments were conducted for various combinations of winning probabilities P_1 , P_2 and P_3 . They were varied between zero and one, with a step size of 0.05. In order to simulate all combinations of these values, 9261 ($= 21^3$) simulations would be required. Since a stochastic process was simulated, outcomes were evidently non-deterministic, thus twenty runs per parameter combination were executed, each of them starting from a different random initial spatial configuration.

For all simulations, the model parameters (ϵ, μ, σ) except P_1 , P_2 and P_3 were kept constant. The reproduction rate μ , exchange rate ϵ and selection rate σ were all fixed to 1, which made the mobility lower than the critical threshold (cfr. Section 1.4.3). Consequently, these conditions permitted sustained coexistence, so that we could study the effects of the non-deterministic competition experimentally.

For every run, the grid configuration was stored every ten generations. This provides us with a dataset of thousands of *in silico* evolutions, which comes in handy if we want to investigate other features of the evolution of the grids throughout a simulation, or if we want to match

the analytical approach that will be presented in Chapter 3 with the computational approach discussed in this chapter.

Reducing the simulation time

Simulations were carried out on UGent's High Performance Computer (HPC). The computational resources (Stevin Supercomputer Infrastructure) and services used in this thesis were thus provided by the VSC (Flemish Supercomputer Center), funded by Ghent University, the Hercules Foundation and the Flemish Government department EWI. Since the required computing time would be quite long, optimizing the code, written in Mathematica (Version 10.0, Wolfram Research Inc., Champaign, USA), would be very beneficial.

Significant gains in required computing time originated from making the code shorter and more straightforward, using the most efficient built-in Mathematica functions and ensuring that unnecessary calculations were avoided. The main reduction in computing time, however, was achieved by acknowledging the symmetry in the interaction scheme. This can be understood by investigating the two competition schemes depicted in Figure 2.3. Suppose that by carrying out simulations we know that for competition scheme (a) species A will be the sole survivor after 10 000 generations. Then, we can say that for scheme (b), which has the same winning probabilities as scheme (a) but cyclically permuted, species B will be the sole survivor after 10 000 generations with high probability.

Relying on this symmetry we only needed to conduct 1561 simulations to obtain results for the entire parameter space. This is only slightly more than one sixth of the original number of simulations that was required (9 261), a significant reduction in the computing costs. If one were to simulate all 1561 simulations on a single core, about 102 hours of computing time would be required. The HPC, however, allowed us to use multiple cores at once, reducing the calculation time to about one hour.

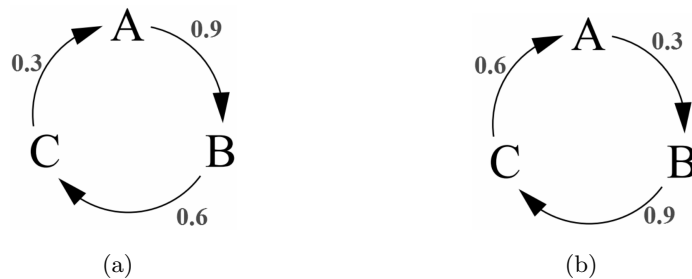


Figure 2.3: Two competition schemes with cyclically permuted winning probabilities: $P_1 = 0.9$, $P_2 = 0.6$, $P_3 = 0.3$ (a), $P_1 = 0.3$, $P_2 = 0.9$, $P_3 = 0.6$ (b)

2.3 Simulation results

2.3.1 The parameter space

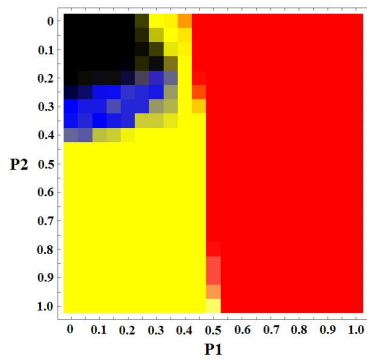
The results of the simulations give us an idea of the region in the parameter space where the species still coexist after 10 000 generations, which we name the region of coexistence, or where a certain species kills off the other two. The results are visualised in the end-state parameter space (Figure 2.4). Black represents the region of coexistence, red represents survival of species A, blue survival of species B and yellow survival of species C. The simulations were conducted twenty times for all required combinations of winning probabilities in the parameter space, starting from a different random initial configuration. The results shown are the outcomes for each combination of winning probabilities, averaged over the twenty simulations. As the end-state parameter space is three dimensional, each figure represents a slice of this space, taken at a height determined by the value P_3 .

From these results, one can state that the region of coexistence can be found where the winning probabilities are of similar magnitudes. In order to have a better insight into how the *in silico* populations vary over time, their temporal evolutions are highlighted for four points in the parameter space in Figures 2.5-2.8. Each figure shows the competition scheme and the evolution of the species' densities through time on a regular plot and on the simplex. Also, an indication of the spatio-temporal evolution is given by the lattice configurations at three instances in time for each of the considered parameter combinations.

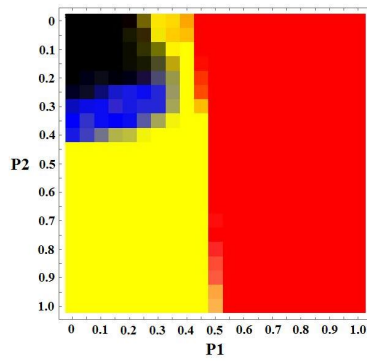
To obtain a trajectory on the simplex, at every instance in time a state in the three-dimensional phase space is projected onto the two-dimensional simplex. A point on the simplex is closer to one of the vertices a , b or c as the relative density of the corresponding species is higher. In the extreme case, when a point is on a vertex, two species went extinct, and the remaining species' name is on the concerned vertex. When one species goes extinct, the trajectory has reached the edge of the simplex, from where it will move towards one of the two vertices on the edge, indicating the extinction of a second species.

Note how this projection from three to two dimensions implies a loss of information. Indeed, whereas it is possible in three-dimensional space to calculate the density of empty cells, this is not possible from the information found on the simplex. Nevertheless, the simplex is an informative way of visualising the dynamics of *in silico* ecosystems.

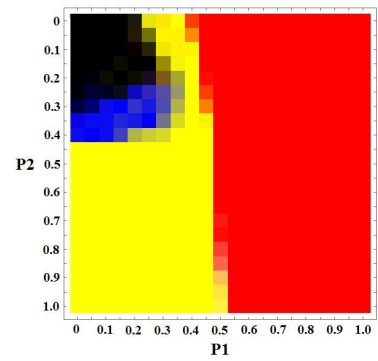
Figure 2.5 shows the evolution of the *in silico* populations for $P_1 = P_2 = P_3 = 0$ up to the 1000th generation. Note that this implies that species B beats species A with probability 1, and so on. Thus, this competition scheme represents deterministic competition, and looks exactly like the scheme in Figure 1.1, but with the direction of the arrows reversed. The



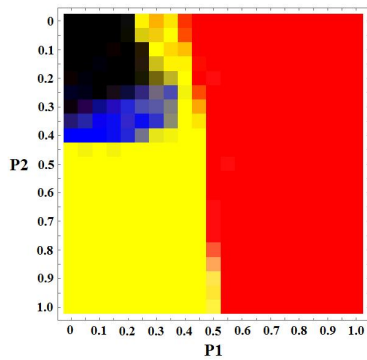
(a) $P_3 = 0$



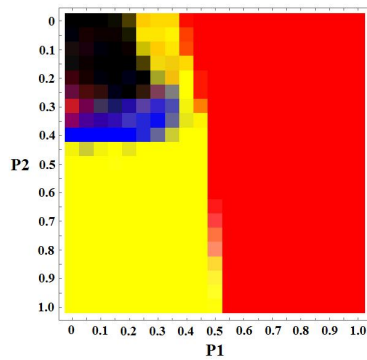
(b) $P_3 = 0.05$



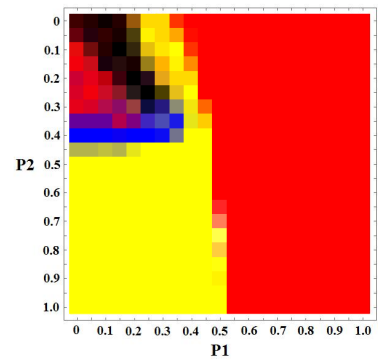
(c) $P_3 = 0.10$



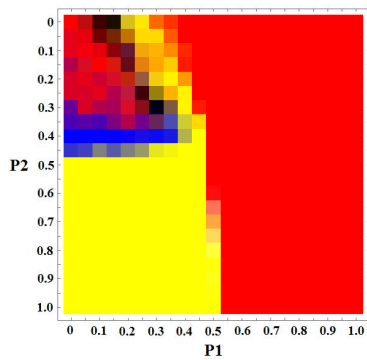
(d) $P_3 = 0.15$



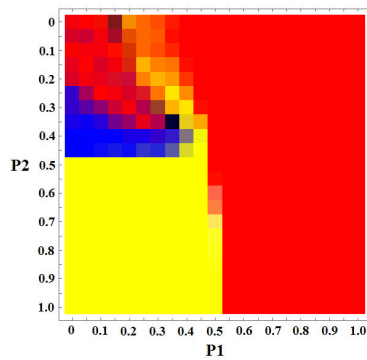
(e) $P_3 = 0.20$



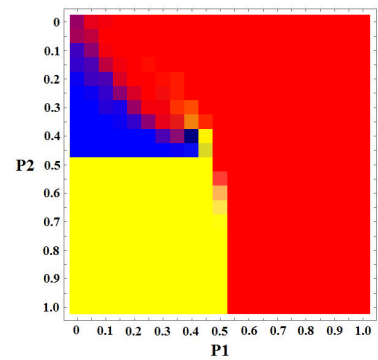
(f) $P_3 = 0.25$



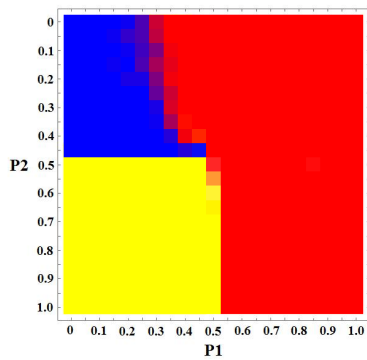
(g) $P_3 = 0.30$



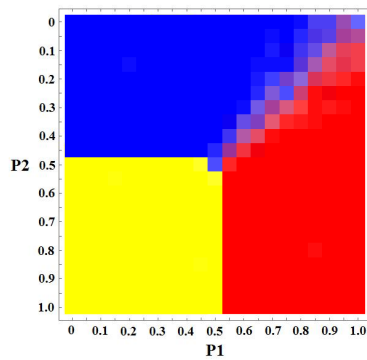
(h) $P_3 = 0.35$



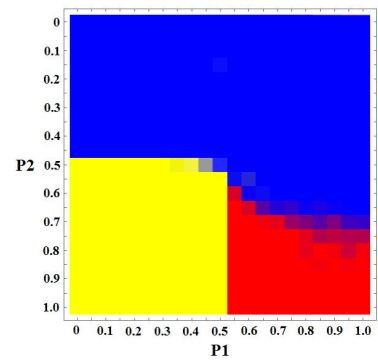
(i) $P_3 = 0.40$



(j) $P_3 = 0.45$



(k) $P_3 = 0.50$



(l) $P_3 = 0.55$

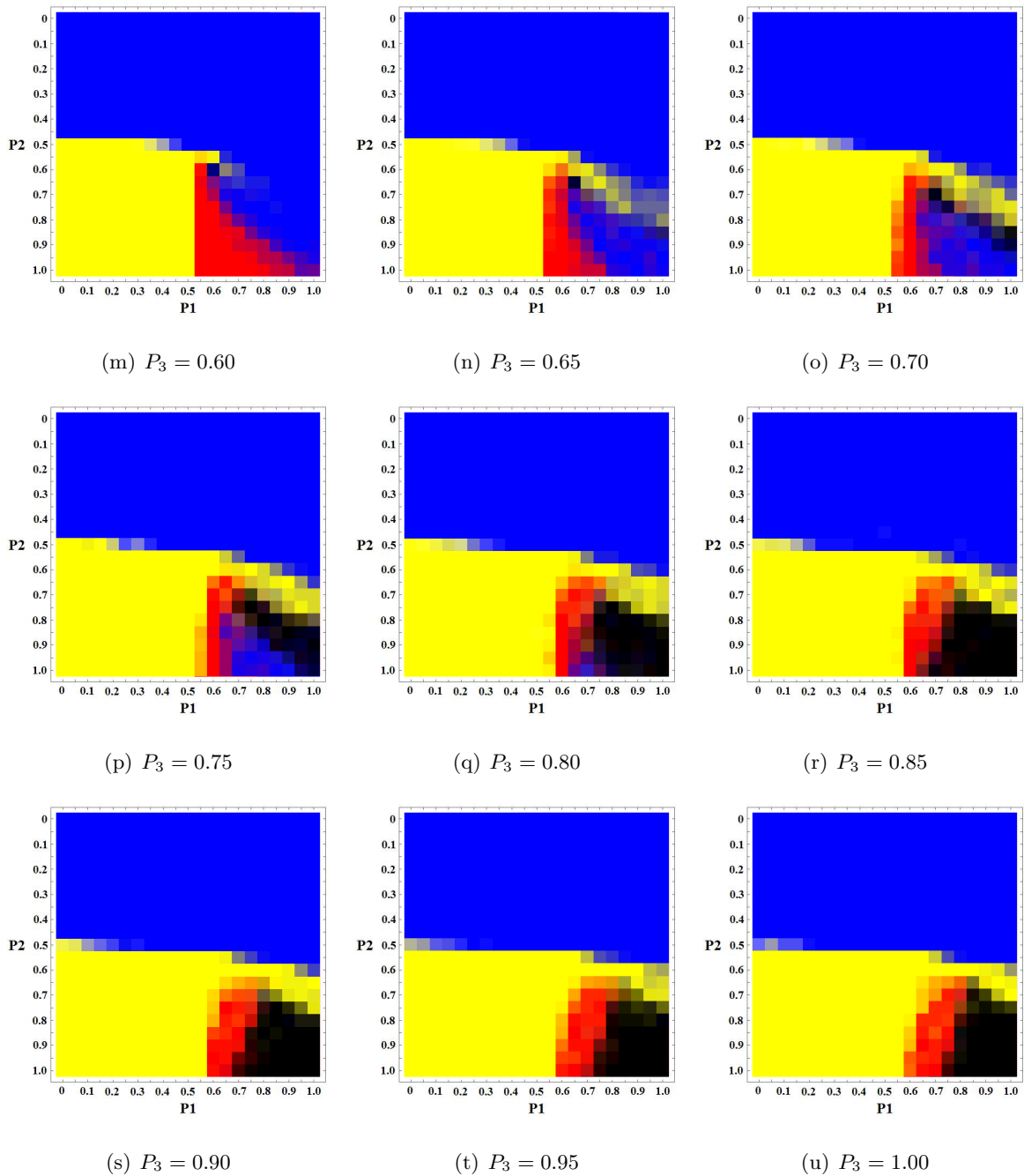


Figure 2.4: The end-state parameter space resulting from the IBM simulations. Black represents the region of coexistence, red represents survival of species A, blue survival of species B and yellow survival of species C, and this state was determined after 10 000 generations. P_3 increases in increments of 0.05 for every subsequent image. P_1 and P_2 vary between zero and one on the x- and y-axis, respectively.

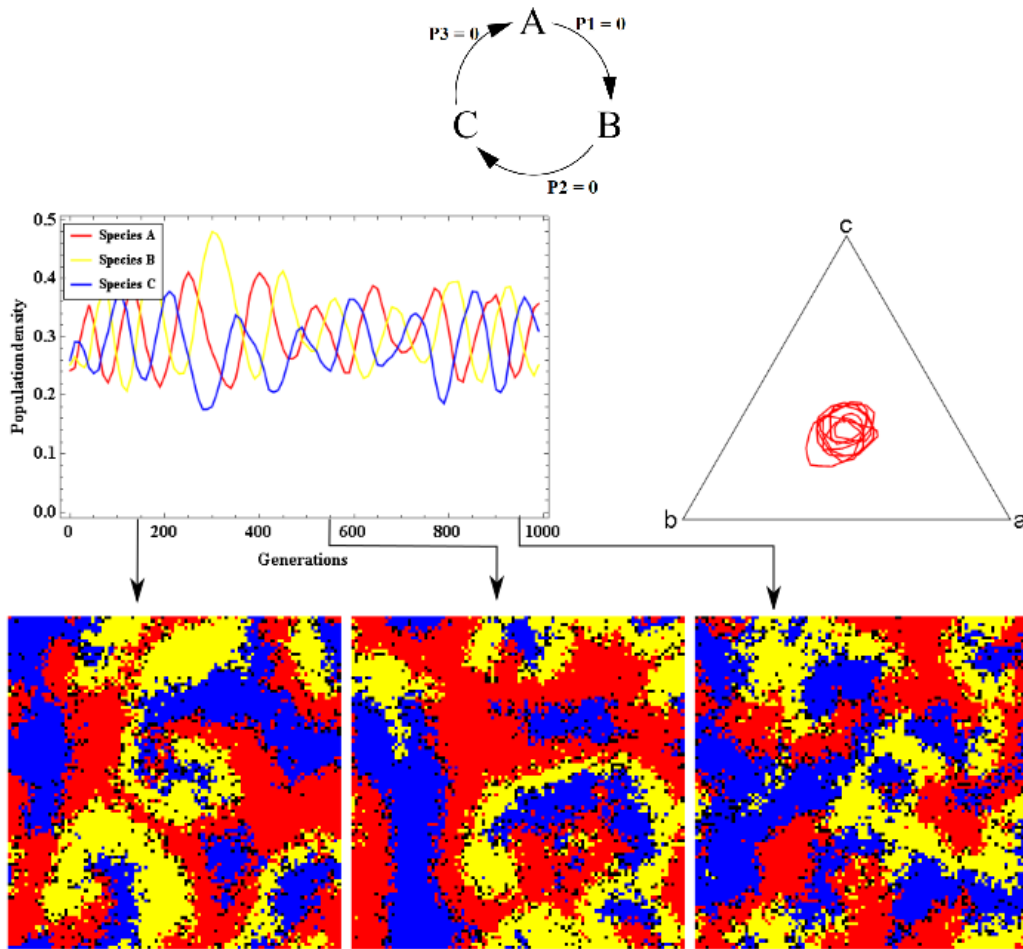


Figure 2.5: The species densities during an IBM simulation with $P_1 = P_2 = P_3 = 0$ are plotted through time on a regular plot and on the simplex, while the spatial configuration is displayed at three instances in time.

species' densities oscillate over time with a small amplitude around equilibrium values that are almost equal for all species, indicating that they coexist in roughly equal proportions. The trajectory on the simplex lies in the centre of the triangle, at relatively large distance from the edges that correspond to extinction of one and eventually two species. On the lattice configurations, spiral waves can be perceived. These are less pronounced than in Figure 1.4 due to the fact that the simulations leading to Figure 2.4 were carried out on a 100×100 lattice.

In Figure 2.6, the winning probabilities are $P_1 = 0.2$, $P_2 = 0.1$ and $P_3 = 0$ and the *in silico* population sizes are shown for the first 1000 generations. The oscillations demonstrate a larger amplitude and a smaller frequency than in the deterministic case (Figure 2.5). The equilibrium value of species C has shifted to a lower value. On the simplex, we see that the

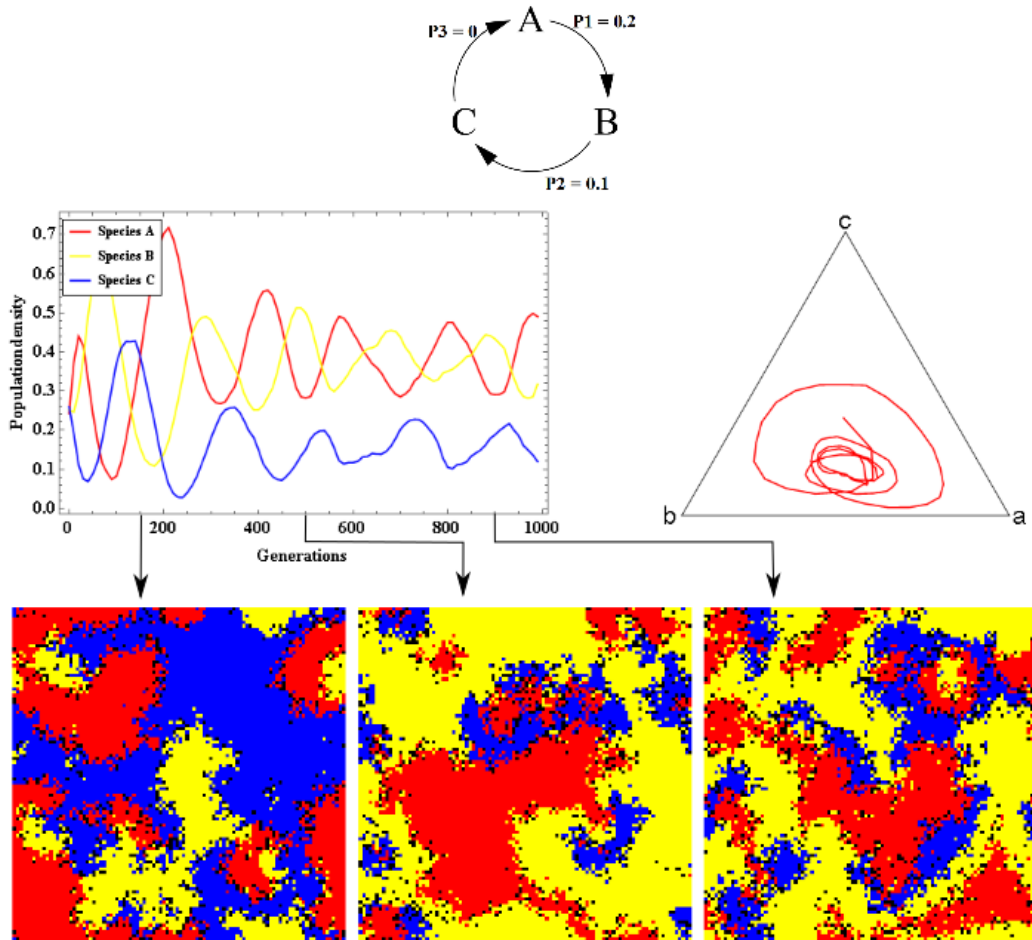


Figure 2.6: The species densities during an IBM simulation with $P_1 = 0.2$, $P_2 = 0.1$ and $P_3 = 0$ are plotted through time on a regular plot and on the simplex, while the spatial configuration is displayed at three instances in time.

trajectory now orbits close to the edge of the triangle. Although coexistence persists during the entire course of the simulation, we anticipate that a larger change in winning probabilities may result in extinction events. On the lattice, although spiral waves still emerge now and then, the IBM has lost its refined configuration as displayed in Figure 2.5 and now shows the balanced chase between large clumps of each species.

In Figure 2.7, $P_1 = 0.35$ while P_2 and P_3 are 0.1 and 0, respectively, as was the case for the setting depicted in Figure 2.6. These winning probabilities result in the extinction of species C after 2200 generations, and of species A after 2800 generations. The equilibrium value of species C has decreased for the worse, and the equilibrium value of species A has strongly increased. On the simplex we see that the trajectory eventually reaches the edge, after which species B outcompetes species A, which corresponds to the trajectory ending up

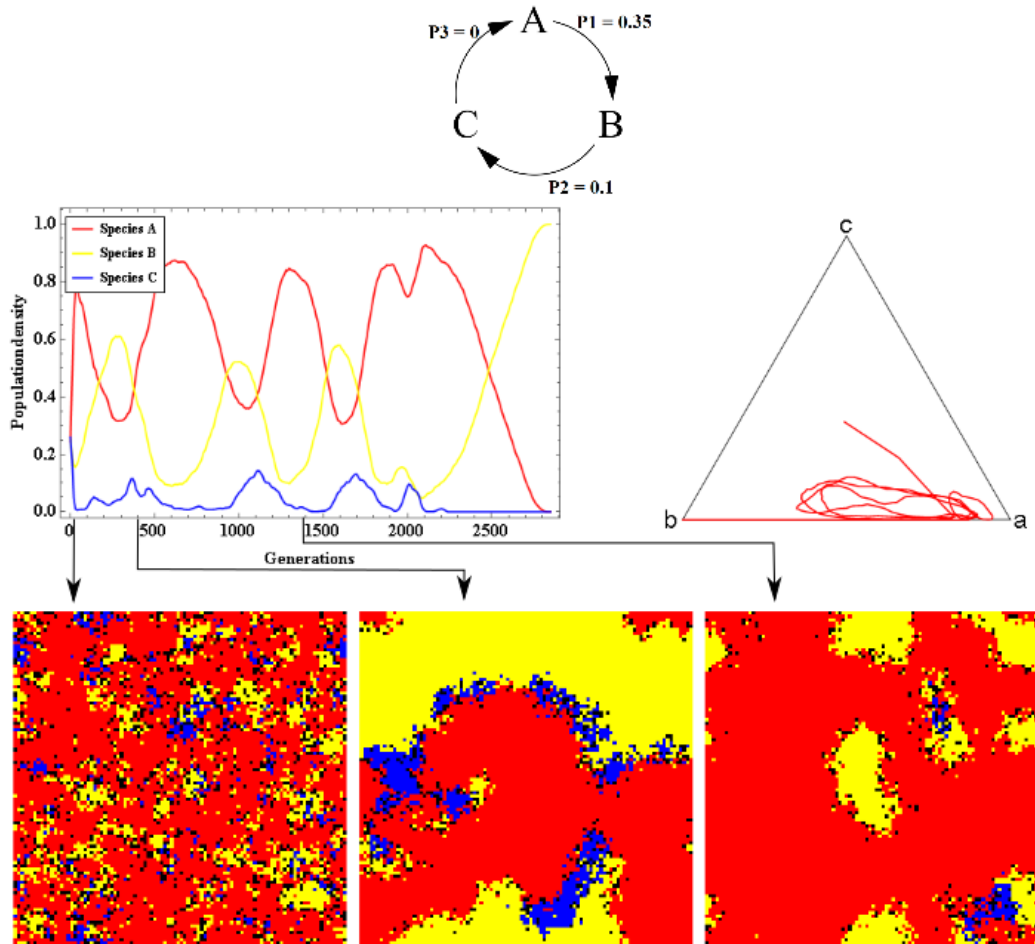


Figure 2.7: The species densities during an IBM simulation with $P_1 = 0.35$, $P_2 = 0.1$ and $P_3 = 0$ are plotted through time on a regular plot and on the simplex, while the spatial configuration is displayed at three instances in time.

on the vertex b . The frequency of the oscillations has decreased once more. On the lattice, the density of species C decreases rapidly during the first 50 generations. After this initial transient, species C manages to organize itself in a thin layer, chasing species B while being chased by species A. Due to this organisation, species C is able to survive for another 2150 generations, after which it finally goes extinct. Note how species A signs its own death warrant by driving species C to extinction, as species B now easily beats species A.

In Figure 2.8, with $P_1 = 0.45$, a trajectory develops where species A is the sole survivor after only 120 generations. This seemingly happens without the species' densities oscillating. Species B and C's densities are seriously reduced after 30 generations. Although species B has a slightly higher probability of defeating species A during a competition event, species B goes extinct due to the high density of species A.

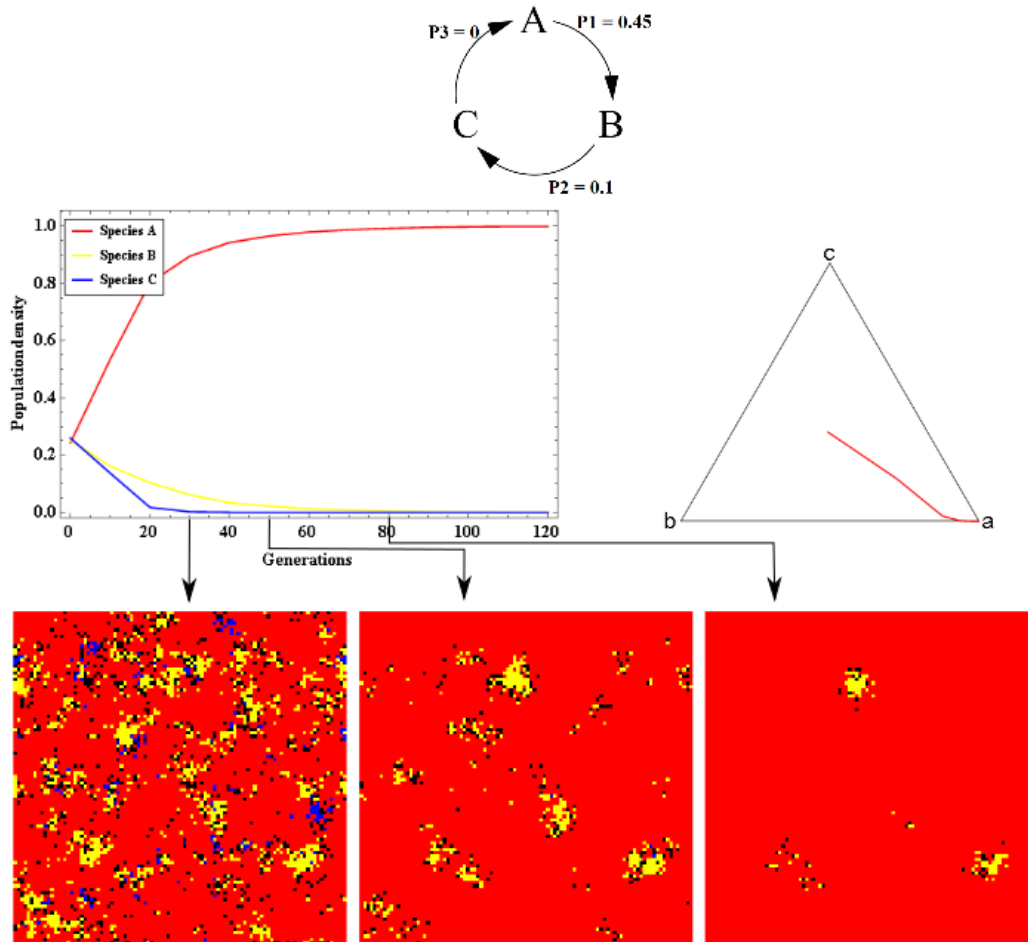


Figure 2.8: The species densities during an IBM simulation with $P_1 = 0.45$, $P_2 = 0.1$ and $P_3 = 0$ are plotted through time on a regular plot and on the simplex, while the spatial configuration is displayed at three instances in time.

2.3.2 Mobility

As stated in Section 1.4.3, Reichenbach et al. (2007) showed that sustained coexistence does not occur when mobility is higher than a certain threshold. This can be explained by realising that when mobility becomes higher, the system's behaviour approximates that of a well-mixed system. Under these circumstances, spatial patterns are not or barely developed, which shortens the duration of coexistence considerably (Laird, 2014).

Thus, in the context of non-deterministic competition, we expect the region of coexistence to shrink when mobility is increased. The end-state parameter space shown in Figure 2.4 is the result of simulations conducted with $\epsilon = 1$. Reichenbach et al. (2007) showed that the mobility, defined as the average area explored by one individual per unit of time, can

be calculated using $M = 2\epsilon/N$, with N the number of cells in the grid. Thus, with $\epsilon = 1$, $M = 2 \times 10^{-4}$ on the 100×100 lattice considered in our experiments. For a mobility higher than the critical mobility $M_c \approx 4,5 \pm 0.5 \times 10^{-4}$, Reichenbach et al. (2007) found that sustained coexistence becomes unlikely to occur.

Similar simulations to the ones presented in Section 2.3.1 were conducted for $\epsilon = 2.25$, which increases the mobility to the critical threshold. Five simulations, starting from a different random initial configuration, were carried out for every combination of winning probabilities, and the average outcomes are given in Appendix A, Figure A.1. The *in silico* behaviour across the end-state parameter space looks similar to the behaviour in Figure 2.4, but the region of coexistence is smaller. For slightly higher mobilities, the region will disappear entirely.

After the death of one species, the remaining two species compete to become the sole survivor. The outcome of this competition is determined by the winning probability between these two species, and their relative abundance when the third competitor is eliminated. Usually, the competition between the remaining two species is settled quickly, but not when the two species kill each other with a probability of 0.5, as the outcome in that case is the result of fluctuations due to the finite size of the grid (Reichenbach et al., 2006). It is hard to notice this in Figure 2.4, as there usually was almost always either coexistence or a sole survivor after 10 000 generations, but this is not the case when mobility is increased. In Figure A.1, white spots are clearly shown, for instance at $P_1 = 0.5$, $P_2 = 1$ and $P_3 = 0.1$. This signifies that after 10 000 generations, two species were still busy settling their fight.

In order to explain why this phenomenon seems to be more articulated for high mobilities, more research is required. For starters, one could conduct several IBM simulations involving two species with winning probability 0.5 until one species goes extinct, and this for different mobilities. This then can result in a curve displaying the relationship between mobility and the time until extinction. Some simulations like these were carried out on a small scale, with a resulting curve that looked quite irregular. It can thus be concluded that explaining the relationship between mobility and the time until extinction may be an elaborate task. Since other aspects of non-deterministic competition seemed more important to research, it was decided that further investigations about the competition between two species with winning probability 0.5 are beyond the scope of this thesis.

2.3.3 Number of generations until one species survives

Figure 2.9 shows the number of generations that were required for a single species to become the sole survivor, as a function of P_1 , P_2 and P_3 , while ϵ is either equal to 1 or 2.25. Since the simulations ran for at most 10 000 generations, this is the maximum value displayed on the figure, although coexistence could persist for more than 10 000 generations in some cases. For

most parameter combinations, two species go extinct soon. However, this changes abruptly once parameter values approach the region of coexistence as given in Figure 2.4. One can thus state that a small change in winning probabilities can have a disastrous effect on the duration of coexistence. The figure also confirms the findings of Section 2.3.2. The region of coexistence is smaller for higher mobility, and at $P_1 = 0.5$, it takes a long time for the two remaining species to settle the fight.

2.4 Discussion

2.4.1 Bifurcations

In dynamical systems, a small change of a parameter value that results in a qualitative change of the system's behaviour is called a bifurcation (Strogatz, 1994). In the context of non-deterministic competition, a change in winning probabilities might determine the stable state the system ends up in, and thus whether species A, B or C becomes the sole survivor. These qualitative changes are essentially bifurcations. Whether the transition from the region of coexistence to extinction is a bifurcation, is hard to predict with the information we have at this point. We do not expect coexistence to be a stable state for any set of winning probabilities. What we call the region of coexistence is probably a set of parameter values for which it takes a long time (more than 10 000 generations) to reach a stable state where only one species survives. However, the sudden drop in the number of generations for which the species manage to coexist, as shown in Figure 2.9, might indicate a bifurcation. Another bifurcation may arise when the oscillations that usually appear in our system suddenly disappear for certain parameter combinations (Figure 2.8). It may be possible to confirm some of these presumptions by investigating the IBM analytically. This will be carried out in Chapters 3 and 4.

2.4.2 Survival of the weakest?

The original observation

Reactions (1.1) are often slightly adapted in such a way that competition and reproduction are combined. It is then assumed that a victory in competition results in an increased reproduction ability, such that both processes actually occur at once. The corresponding reactions are given by

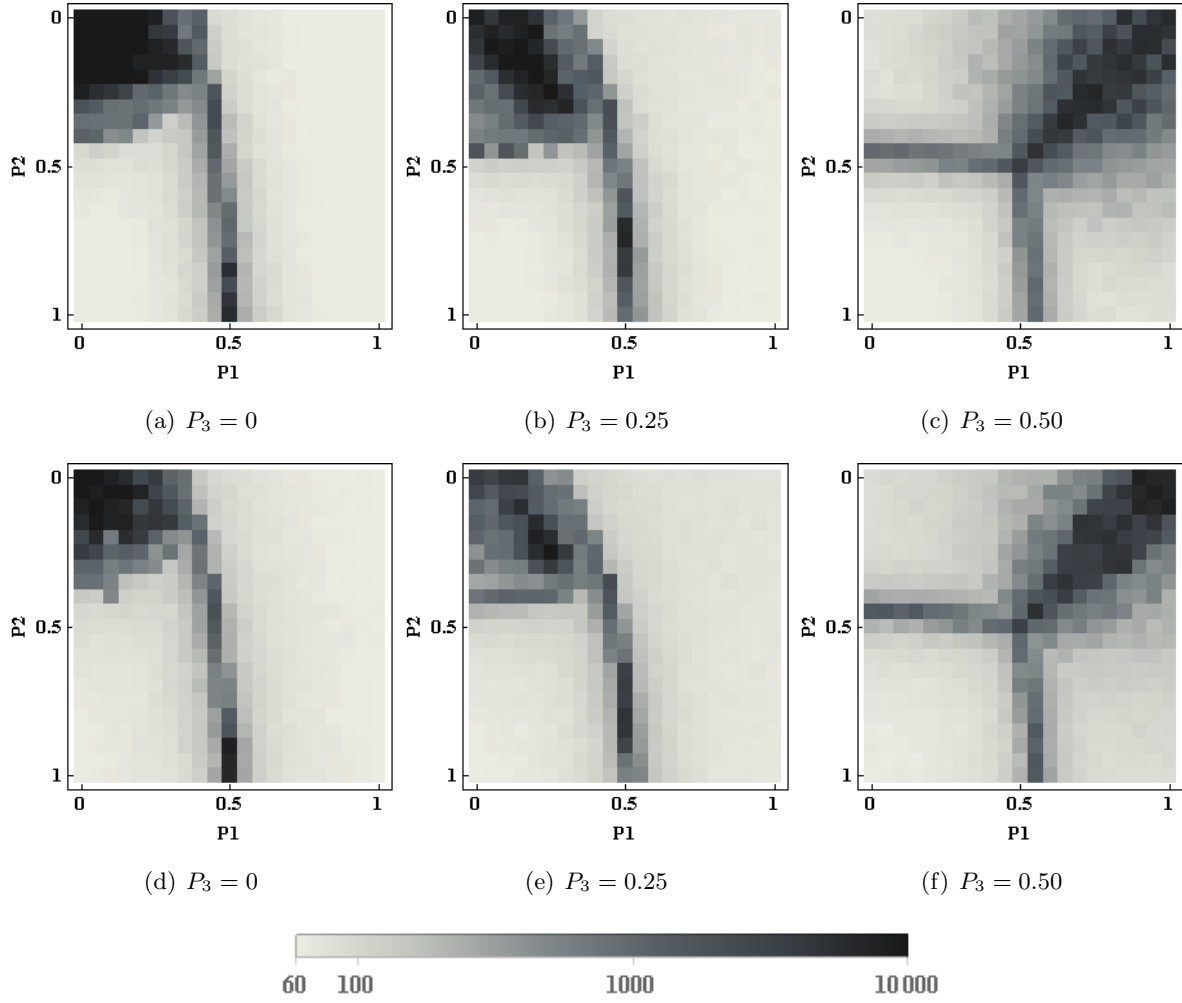


Figure 2.9: The number of generations that were required for a single species to become the sole survivor, with $\epsilon = 1$ (a, b, c) or $\epsilon = 2.25$ (d, e, f).



where species A outcompetes species B and reproduces at invasion rate k_A , and similarly for the other reactions. The mean-field equations of this system are then given by

$$\begin{cases} \dot{a} = a[k_A b - k_C c], \\ \dot{b} = b[k_B c - k_A a], \\ \dot{c} = c[k_C a - k_B b], \end{cases} \tag{2.2}$$

and exhibit a slightly different dynamics than that of System (1.2). The fixed point corresponding to coexistence becomes $\frac{1}{k_A+k_B+k_C}(k_B, k_C, k_A)$ and is neutrally stable, and therefore surrounded by neutrally stable closed orbits which allow for sustained coexistence with oscillating species densities. Most noticeable about the fixed point, however, is that the populations of the species are not determined by their own invasion rate but by the rates of the species they outcompete, as at the fixed point corresponding to coexistence the density of species A, for instance, is equal to $\frac{k_B}{k_A+k_B+k_C}$.

Now, imagine that species A's invasion rate k_A was lowered, then the population density of species C at the fixed point would shift to a lower value, while the density of species A would increase. This makes species A the least probable species to go extinct in a stochastic simulation, a counter-intuitive result (Frean and Abraham, 2001). Of course, these conclusions are only valid when the mean-field assumptions are satisfied, but even in IBM simulations in two-dimensional space a decrease in invasion rate of one species leads to a higher probability of the other two becoming extinct. This phenomenon was named the "survival of the weakest" (Frean and Abraham, 2001).

Comparison with winning probabilities

The main conclusion that can be drawn from the simulations for our system is that coexistence persists where the three winning probabilities are of similar magnitudes. Sustained coexistence is more likely to occur where all three winning probabilities are either low or high, and intermediate values seem less likely to lead to sustained coexistence.

This is the result one should expect considering the competition scheme with a set of specific winning probabilities. If a certain species kills the other two with relatively high probability, this species will eventually dominate the system, and remain as the sole survivor. When it holds that for each species the probability of outcompeting is similar to the probability of being outcompeted, sustained coexistence is more likely to occur.

This outcome seems to contradict the study carried out by Frean and Abraham (2001). But this is a mere consequence of the fact that the rules governing the species in their model are slightly different from the ones in our adaptation. While the strongest is defined as the species with the highest reaction rate in the system by Frean and Abraham (2001), it is the one with the highest probability of winning from the others that is considered the strongest in our setting. One may therefore be inclined to relax the term "survival of the weakest" to "survival of the least aggressive", and reinstate "survival of the strongest" as a result from the simulations carried out in this thesis.

CHAPTER 3

Towards an analytical description of in silico microbial dynamics

The computational approach presented in Chapter 2 allowed us to gain some insight into how the behaviour of the IBM with non-deterministic cyclic competition changes across the parameter space. But there is a black box feeling to our endeavours. Despite knowing where the region of coexistence lies, this is only an approximation, and moreover we do not know why a certain set of winning probabilities allows for sustained coexistence, and another set does not. Obtaining more precise, and possibly analytical results would increase our knowledge and understanding of the system's behaviour. The best possible result to obtain would be a closed-form expression for the region of coexistence in the parameter space, as a function of the winning probabilities. Trying to obtain this result, we will explore modelling approaches in this chapter that allow us to approximate the behaviour of the IBM, but that are simpler and thus possibly allow for obtaining analytical results. Some of these modelling approaches have already been introduced in Section 1.4, while others will be introduced in this chapter. Models that are more closely related to the IBM will be introduced first, while models built upon a continuous time, space or state domain will be discussed last.

3.1 Every possible interaction

The IBM used in Chapter 2 has two sources of stochasticity. Firstly, the initial configuration of the grid is constructed at random. Secondly, at every step a random individual is selected to interact with a random neighbour, and the type of interaction is selected randomly. The idea of the model proposed in this section is to eliminate the randomness as a consequence of the interaction processes, so that the outcome of a model simulation is completely determined by the initial condition and the rules applied to the individuals. In this way, at every consecutive time step, every individual will interact with each neighbour through every possible interaction at once.

In this setting, every grid cell can be characterised by three numbers, rather than one. Each number stands for the probability that the individual in that cell belongs to species A, B or C. The grid is initialised in a similar way as in the case of the IBM model, but now the states of the cells are either $(1, 0, 0)$, $(0, 1, 0)$, $(0, 0, 1)$ or $(0, 0, 0)$, reflecting a 100% chance of containing an individual of species A, B or C, or of being empty, respectively. After the initialisation, the grid is updated. During the evolution, every cell on the grid is assigned three new values at every consecutive time step, and this happens synchronously. The new states are calculated using formulae based on the probability of selecting an individual, of selecting a neighbour and of selecting an interaction.

Adopting notation from graph theory (Bondy and Murty, 2008), let us denote the probability of finding a member of species A in cell k as P_A^k , and similarly for species B and C. Then

$$\begin{aligned}
P_A^k(t+1) &= \underbrace{P_A^k(t)}_1 \\
&+ \frac{1}{N^D} \left(\underbrace{\frac{\epsilon/\xi}{|N_k|} [1 - P_A^k(t)] \sum_{l \in N_k} P_A^l(t)}_{2(a)} - \underbrace{\frac{\epsilon/\xi}{|N_k|} P_A^k(t) \sum_{l \in N_k} [1 - P_A^l(t)]}_{2(b)} \right. \\
&\quad \left. - \underbrace{\frac{\sigma/\xi}{|N_k|} P_A^k(t) \sum_{l \in N_k} [P_3 P_C^l(t) + (1 - P_1) P_B^l(t)]}_{2(c)} \right. \\
&\quad \left. + \underbrace{\frac{\mu/\xi}{|N_k|} [1 - P_A^k(t) - P_B^k(t) - P_C^k(t)] \sum_{l \in N_k} P_A^l(t)}_{2(d)} \right) \quad (3.1) \\
&+ \underbrace{\sum_{l \in N_k} \frac{1}{N^D} \left(\frac{\epsilon/\xi}{|N_l|} P_A^l(t) [1 - P_A^k(t)] - \frac{\epsilon/\xi}{|N_l|} [1 - P_A^l(t)] P_A^k(t) \right.}_{3} \\
&\quad \left. - \frac{\sigma/\xi}{|N_l|} [P_3 P_C^l(t) + (1 - P_1) P_B^l(t)] P_A^k(t) \right. \\
&\quad \left. + \frac{\mu/\xi}{|N_l|} P_A^l(t) [1 - P_A^k(t) - P_B^k(t) - P_C^k(t)] \right),
\end{aligned}$$

with ϵ , σ and μ as defined in Section 1.4.3, $\xi = \epsilon + \sigma + \mu$ and P_1 and P_3 as in Section 2.2.1, N^D the number of cells in a D -dimensional lattice, and $|N_k|$ the number of cells l in the neighbourhood N_k of cell k . Similar equations can be constructed for $P_B^k(t+1)$ and $P_C^k(t+1)$, but they are omitted for the sake of brevity.

Since a von Neumann neighbourhood is used for the two-dimensional IBM simulations, we have $|N_k| = |N_l| = 4$ (Von Neumann and Burks, 1966). The neighbours of cell k are then the elements of the set $\{l_1, l_2, l_3, l_4\}$, as displayed in Figure 3.1.

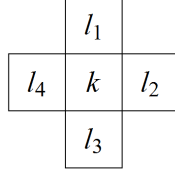


Figure 3.1: The neighbours of cell k in a von Neumann neighbourhood are the elements of the set $\{l_1, l_2, l_3, l_4\}$.

The right hand side of Eq. (3.1) has three terms, two of which consist of four parts. They can be understood as follows:

1. The probability of finding species A in cell k at time t ;
2. The probability that cell k is randomly selected to interact is $\frac{1}{N^D}$. The probability of finding species A in cell k can then be changed by an interaction, in the following ways:
 - (a) An individual of species A from a neighbouring cell l takes part in an exchange event with an individual of species B or C, or an empty space, in cell k . The probability of such an exchange event is ϵ/ξ . The probability that cell k is not inhabited by species A is $[1 - P_A^k(t)]$, while $P_A^l(t)$ is the probability that a neighbouring cell l is inhabited by species A. This neighbouring cell is selected for interaction with cell k with probability $\frac{1}{|N_k|}$. Since every neighbour l can be selected for interaction, a summation over all these neighbours is necessary;
 - (b) An individual of species A leaves cell k by exchanging its place with a neighbour in l that is not A. Everything is similar to the previous term, except that it is now required that cell k is inhabited by species A and its neighbours l are not inhabited by species A;
 - (c) An individual of species A in cell k is killed by its adversary in a neighbouring cell l . Cell k is inhabited by species A with probability $P_A^k(t)$, and selection occurs with probability σ/ξ . The individual in cell l then kills species A in k . Again, summation over all neighbours is necessary, and a certain neighbour is selected with probability $\frac{1}{|N_k|}$;
 - (d) When cell k is empty, it is possible that an individual of species A in a cell l produces offspring that is placed in its neighbouring cell k . The probability of cell k being empty is $[1 - P_A^k(t) - P_B^k(t) - P_C^k(t)]$ and the probability that cell l is inhabited by species A is $P_A^l(t)$;

3. The third term works the other way around. One of the neighbouring cells l is selected first, and subsequently interacts with a neighbour which happens to be cell k . This term thus is the sum over all cells l that can be selected, which happens with probability $\frac{1}{N^D}$. The components of this term are very similar to those in term two. Cell l has a probability $\frac{1}{|N_l|}$ of selecting cell k to interact with. Based on the species in cells l and k , the results of the possible interactions are calculated.

Eq. (3.1) is now simplified and restricted to a two-dimensional lattice, where $|N_k| = |N_l| = 4$, as in the IBM simulations. If we further denote $P_A^k(t) + P_B^k(t) + P_C^k(t)$ by $P_T^k(t)$, we obtain P_A^k , P_B^k and P_C^k at time $(t + 1)$ as follows:

$$\left\{ \begin{array}{l} P_A^k(t+1) = \left(1 - \frac{1}{2N^2\xi} \left[4\epsilon - \sigma \left(P_3 \sum_{l \in N_k} P_C^l(t) + (1 - P_1) \sum_{l \in N_k} P_B^l(t) \right) \right] \right) P_A^k(t) \\ \quad + \frac{1}{2N^2\xi} \left(\epsilon + \mu [1 - P_T^k(t)] \right) \sum_{l \in N_k} P_A^l(t), \\ P_B^k(t+1) = \left(1 - \frac{1}{2N^2\xi} \left[4\epsilon - \sigma \left(P_1 \sum_{l \in N_k} P_A^l(t) + (1 - P_2) \sum_{l \in N_k} P_C^l(t) \right) \right] \right) P_B^k(t) \\ \quad + \frac{1}{2N^2\xi} \left(\epsilon + \mu [1 - P_T^k(t)] \right) \sum_{l \in N_k} P_B^l(t), \\ P_C^k(t+1) = \left(1 - \frac{1}{2N^2\xi} \left[4\epsilon - \sigma \left(P_2 \sum_{l \in N_k} P_B^l(t) + (1 - P_3) \sum_{l \in N_k} P_A^l(t) \right) \right] \right) P_C^k(t) \\ \quad + \frac{1}{2N^2\xi} \left(\epsilon + \mu [1 - P_T^k(t)] \right) \sum_{l \in N_k} P_C^l(t). \end{array} \right. \quad (3.2)$$

After initialising the grid, System of Equations (3.2) can be applied to every cell simultaneously. Note that N^2 updates are necessary to evolve one generation.

Mimicking the IBM simulations by means of System (3.2) would definitely be interesting, as the evolution of the grid would then be deterministic. Unfortunately, there is a flaw in the reasoning leading to them. This can be illustrated by considering the following very simple system. A one-dimensional space made up of three cells, with periodic boundary conditions, is inhabited by one species. The species can only reproduce, meaning that $\mu = 1$ while $\epsilon = \sigma = 0$. Then, we can construct the counterpart of System (3.2) for the simple system considered here:

$$P^k(t+1) = P^k(t) + \frac{1}{3} [1 - P^k(t)] \sum_{l \in N_k} P^l(t). \quad (3.3)$$

Let us take $(0, 0, 1)$ as initial condition. The rightmost cell is inhabited by an individual, while the two other cells are empty. In an IBM simulation, one of the three cells will be selected, and then one of the neighbours of this cell will be chosen for interaction. Since $\mu = 1$ and $\epsilon = \sigma = 0$, the type of interaction will always be reproduction. Thus, from this initial condition, six possible transitions can occur as the result of one interaction in the IBM, each with probability $\frac{1}{6}$:

$$\begin{array}{l}
 (0, 0, 1) \xrightarrow{\frac{1}{6}} (1, 0, 1) \\
 \xrightarrow{\frac{1}{6}} (0, 0, 1) \\
 \xrightarrow{\frac{1}{6}} (0, 0, 1) \\
 \xrightarrow{\frac{1}{6}} (0, 1, 1) \\
 \xrightarrow{\frac{1}{6}} (0, 1, 1) \\
 \xrightarrow{\frac{1}{6}} (1, 0, 1)
 \end{array}$$

The results of these transitions reduce to three configurations, each of them occurring with probability $\frac{1}{3}$. Taking the sum over these configurations, we obtain the probabilities of finding an individual in each of the cells, i.e. $(\frac{1}{3}, \frac{1}{3}, 1)$. These probabilities also follow from using System (3.3). The three configurations can now undergo another reproduction interaction in the IBM, resulting in the following possible transitions:

$$\begin{array}{l}
 (1, 0, 1) \xrightarrow{\frac{1}{3}} (1, 0, 1) \\
 \xrightarrow{\frac{2}{3}} (1, 1, 1) \\
 \\
 (0, 0, 1) \xrightarrow{\frac{1}{3}} (0, 0, 1) \\
 \xrightarrow{\frac{1}{3}} (1, 0, 1) \\
 \xrightarrow{\frac{1}{3}} (0, 1, 1) \\
 \\
 (0, 1, 1) \xrightarrow{\frac{1}{3}} (0, 1, 1) \\
 \xrightarrow{\frac{1}{3}} (1, 1, 1)
 \end{array}$$

From this, it follows that the probabilities of finding an individual in each of the cells after two interactions is $(\frac{2}{3}, \frac{2}{3}, 1)$ for the IBM. However, applying Eq. (3.3) twice to initial condition $(0, 0, 1)$ yields $(\frac{17}{27}, \frac{17}{27}, 1)$, a slight underestimate. This is because Eq. (3.3) interprets the probabilities after one interaction, i.e. $(\frac{1}{3}, \frac{1}{3}, 1)$, wrongly. The equation assumes that the

probability of the configuration where both the leftmost cell and the central cell are inhabited by an individual is $\frac{1}{3} \times \frac{1}{3} = \frac{1}{9}$. From writing out the first interaction in an IBM simulation explicitly, however, we see that the probability of this configuration is zero after one interaction, since then the individual in the rightmost cell would have to reproduce both in the leftmost and the central cell during one interaction. System (3.2) is thus too simple to exactly describe the nature of an IBM simulation.

Interestingly, on a two-dimensional grid, spiral waves emerge when an initial configuration is evolved according to System (3.2). When they are applied in one dimension, travelling waves and irregular behaviour occur, two phenomena that we will also encounter in Chapter 4. Thus, although not entirely correct, the equations seem to embody behaviour that is very similar to the behaviour of the IBM. It would therefore be interesting to research the magnitude of the error introduced by the equations. However, this is beyond of the scope of this thesis. We have thus not used System (3.2) to obtain more information on the behaviour of the IBM, and have instead resorted to other, more established models.

3.2 Coupled map lattice

In a coupled map lattice, space and time are discrete, while the state of the spatial entities is continuous (Kaneko, 1993). Space is divided into cells, much like in the IBM, and the dynamics in each cell is governed by a recursion relation, called a map. The logistic map (Verhulst, 1838) is probably the best known example of a map, because of its simple formulation and its very complicated dynamics (May, 1976). Such a map determines the value of x_{t+1} , based on the value x_t at the previous time step.

A similar map can also be constructed using the rules presented in Section 2.2. Imagine a well-mixed vessel, at time step t , where the three species are present with densities a_t , b_t and c_t , and it holds that $a_t + b_t + c_t = \rho_t \leq 1$ for all t . Following the rules from Section 2.2, some of these species will be killed through competition, whereas reproduction might cause the density of these species to rise. The densities a , b and c after one more time step are thus given by

$$\begin{cases} a_{t+1} = a_t [1 - \sigma(1 - P_1)b_t - \sigma P_3 c_t + \mu(1 - \rho_t)], \\ b_{t+1} = b_t [1 - \sigma(1 - P_2)c_t - \sigma P_1 a_t + \mu(1 - \rho_t)], \\ c_{t+1} = c_t [1 - \sigma(1 - P_3)a_t - \sigma P_2 b_t + \mu(1 - \rho_t)]. \end{cases} \quad (3.4)$$

This three-dimensional map can now be used in every cell of the grid. These cells can subsequently be coupled in order to mimic diffusion. In this way, the densities of the three

species in every cell are compared to the densities in neighbouring cells, so that the number of species migrating to another cell can be calculated.

Although it is possible to analyse coupled map lattices of one-dimensional maps (Kaneko, 1993; Atmanspacher et al., 2005), no analysis involving three-dimensional maps was found in literature. This comes as no surprise, as three-dimensional maps, coupled by diffusion, make the analysis much harder. We therefore decided not to consider coupled map lattices in this thesis any further.

3.3 The mean-field equations

The mean-field equations have already been introduced in Section 1.4.1. They are built upon a continuous state and time. Space, however, is neglected, which might make them an inappropriate tool for understanding the behaviour of the IBM. We will first briefly discuss the dynamics of the mean-field equations with deterministic competition, and we will then state how non-deterministic competition influences this dynamics.

3.3.1 Deterministic competition

The mean-field equations for deterministic competition, given by System (1.2), possess five fixed points. These correspond to the values for a , b and c at which the system is in equilibrium, meaning that the time derivatives in System (1.2) are all equal to zero (De Baets, 2013). The first of them, $\mathbf{x}_1^* = (0, 0, 0)$, is unstable, and represents the situation where no species are present. Three fixed points are saddle points, and each of them signifies the survival of one species: $\mathbf{x}_2^* = (1, 0, 0)$, $\mathbf{x}_3^* = (0, 1, 0)$ and $\mathbf{x}_4^* = (0, 0, 1)$. These three fixed points are connected by a heteroclinic orbit. The fifth fixed point is unstable, and corresponds to the situation where the three species coexist, $\mathbf{x}_5^* = \frac{\mu}{3\mu+\sigma}(1, 1, 1)$.

The phase space for System (1.2) is visualised in Figure 3.2. Fixed points \mathbf{x}_2^* , \mathbf{x}_3^* , \mathbf{x}_4^* and \mathbf{x}_5^* sit on an invariant manifold, illustrated by the grey surface. This manifold is called invariant because trajectories that are on this manifold, stay on this manifold for ever. All trajectories (except for those starting from and thus remaining in \mathbf{x}_1^*) approach the invariant manifold exponentially fast (Zeeman, 1993), since the eigendirection normal to the manifold is stable. Once trajectories are close to the invariant manifold, they spiral away from the unstable coexistence fixed point, and approach the boundary of the invariant manifold. This boundary is the heteroclinic orbit. Trajectories will now remain close to the heteroclinic orbit, yet while travelling through the phase space, repeatedly visiting the neighbourhoods of fixed points \mathbf{x}_2^* , \mathbf{x}_3^* and \mathbf{x}_4^* . This oscillating behaviour will go on for an infinite amount of time, but with increasing cycle duration. The trajectories will thus keep on visiting the

neighbourhoods of fixed points \mathbf{x}_2^* , \mathbf{x}_3^* and \mathbf{x}_4^* , but they will remain in these neighbourhoods for increasingly longer times. The densities of the species will thus oscillate, and the frequency of this oscillation will decline. This is illustrated in Figure 3.3, where the trajectory, after a short transient, ends up in the vicinity of the heteroclinic orbit, causing the species densities to oscillate.

Thus in theory, these trajectories never end up on the heteroclinic orbit, they only approach it ever closer. However, this is an unrealistic scenario for the finite-size population of an IBM, as trajectories of finite-size systems will eventually end up on the heteroclinic orbit, due to fluctuations. This illustrates the somewhat limited applicability of the mean-field equations, as discussed in Section 1.4.1. As a consequence of their underlying assumptions, they only hold for perfectly well-mixed, infinite size systems, and will therefore exhibit a slightly different dynamics compared to the one displayed by the IBM. As an illustration, a trajectory starting off close to the coexistence fixed point is shown in Figure 3.2. After a short transient, it approaches the heteroclinic orbit. Due to finite-size fluctuations, it eventually ends up at fixed point $\mathbf{x}_2^* = (1, 0, 0)$ (Reichenbach et al., 2008).

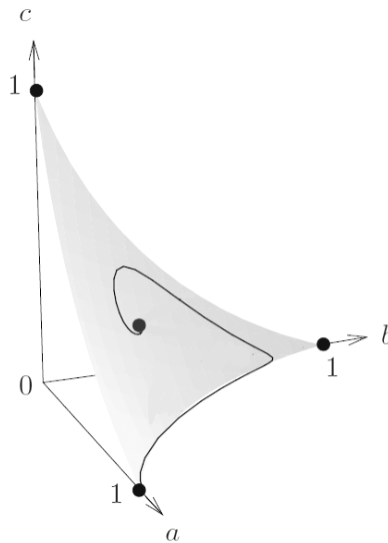


Figure 3.2: The phase space of System (1.2), spanned by the densities a , b and c of species A, B and C. The invariant manifold (grey surface) is shown, with the three fixed points corresponding to survival of one species (on the edges of the grey surface) and the fixed point of coexistence (in the center of the grey surface). The heteroclinic orbit is the boundary of the invariant manifold. A trajectory starting off close to the coexistence fixed point is also displayed (Reichenbach et al., 2008).

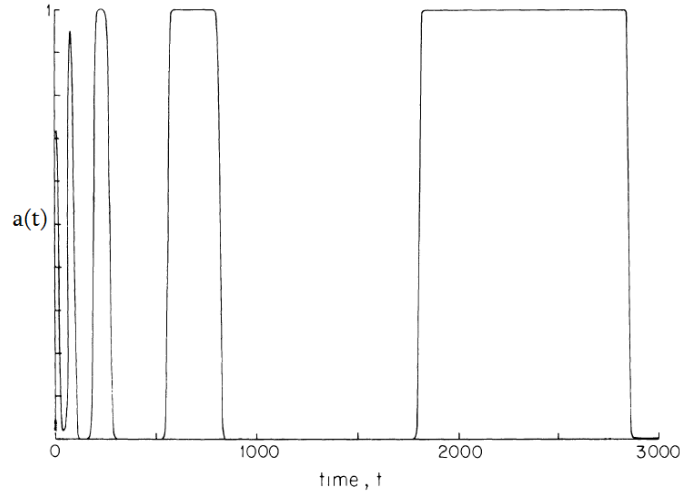
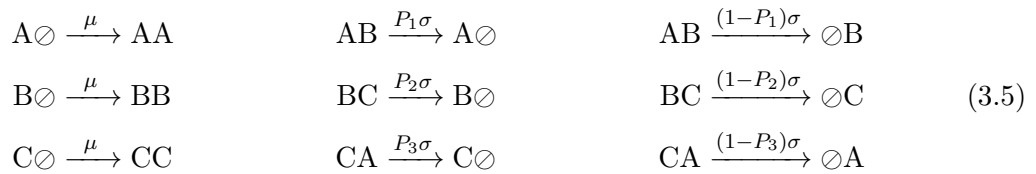


Figure 3.3: Qualitative illustration of how the density of a species A, subject to cyclic competition, varies through time when the trajectory is in the vicinity of the heteroclinic orbit. (May and Leonard, 1975).

3.3.2 Non-deterministic competition

Mean-field equations

In order to derive the mean-field equations for the *in silico* ecosystem governed by non-deterministic competition, we first derive the non-deterministic counterpart of Reactions (1.1). While the reactions modelling reproduction remain unchanged, the selection rate is now modulated by the winning probabilities. The selection rate remains σ , but species A only beats species B at a rate $P_1\sigma$, while B beats A at a rate $(1 - P_1)\sigma$, and so on. The reactions for the non-deterministic system are thus given by



where \emptyset represents an empty site.

Following the reasoning laid out in Section 1.4.1, we derive the mean-field equations for the *in silico* ecosystem governed by non-deterministic competition, based on Reactions (3.5). The change of the density of species A through time, denoted \dot{a} , increases through reproduction and decreases through selection. The difference with the deterministic system is that species

A can now be beaten by both species B and C, and thus both these selection rates should be included. The overall governing system of equations is given by

$$\begin{cases} \dot{a} = \mu a(1 - \rho) - \sigma a [P_3 c + (1 - P_1) b], \\ \dot{b} = \mu b(1 - \rho) - \sigma b [P_1 a + (1 - P_2) c], \\ \dot{c} = \mu c(1 - \rho) - \sigma c [P_2 b + (1 - P_3) a], \end{cases} \quad (3.6)$$

with P_1, P_2 and P_3 the winning probabilities as defined in Figure 2.2.

It is possible to write these equations in a more general form, which clarifies that they are a specific case of the equations investigated by May and Leonard (1975). We rescale time by setting $t^* = \mu t$, and take $k = \sigma/\mu$, to get

$$\begin{cases} \dot{a} = a [1 - a - \beta_1 b - \gamma_1 c], \\ \dot{b} = b [1 - \alpha_1 a - b - \gamma_2 c], \\ \dot{c} = c [1 - \alpha_2 a - \beta_2 b - c], \end{cases} \quad (3.7)$$

with $\beta_1 = 1 + k(1 - P_1)$, $\gamma_1 = 1 + kP_3$, $\alpha_1 = 1 + kP_1$, $\gamma_2 = 1 + k(1 - P_2)$, $\alpha_2 = 1 + k(1 - P_3)$, $\beta_2 = 1 + kP_2$, and where the asterisks were dropped for the sake of brevity.

Fixed points

It is not possible to solve Systems (3.6) and (3.7) analytically, due to their nonlinear nature. However, a more qualitative analysis can provide us with a good understanding of their behaviour.

First of all, we can determine the system's fixed points. We do so by setting $\dot{a} = \dot{b} = \dot{c} = 0$, after which the resulting system of nonlinear algebraic equations can be solved. Since we are interested in the influence of the winning probabilities on the dynamics, we will assume $k = 1$ for simplicity. In contrast to the system considering deterministic competition, System (3.6) has eight fixed points, representing four cases:

1. No species are present:

$$\mathbf{x}_1^* = (0, 0, 0);$$

2. One species is present:

$$\mathbf{x}_2^* = (1, 0, 0),$$

$$\mathbf{x}_3^* = (0, 1, 0),$$

$$\mathbf{x}_4^* = (0, 0, 1);$$

3. Two species are present:

$$\begin{aligned}\mathbf{x}_5^* &= \frac{1}{1 + P_1(1 - P_1)}(1 - P_1, P_1, 0), \\ \mathbf{x}_6^* &= \frac{1}{1 + P_3(1 - P_3)}(P_3, 0, 1 - P_3), \\ \mathbf{x}_7^* &= \frac{1}{1 + P_2(1 - P_2)}(0, 1 - P_2, P_2);\end{aligned}$$

4. Three species are present:

$$\mathbf{x}_8^* = w(a_8^*, b_8^*, c_8^*),$$

with

$$\begin{aligned}w &= (P_1^2 + P_2^2 + (P_3 - 2)^2 + P_2(3P_3 - 4) + P_1(3P_3 + 3P_2 - 4))^{-1}, \\ a_8^* &= P_2^2 + P_2(P_3 + P_1 - 2) - P_1 + 1, \\ b_8^* &= P_3^2 + P_3(P_2 + P_1 - 2) - P_2 + 1, \\ c_8^* &= P_1^2 + P_1(P_3 + P_2 - 2) - P_3 + 1.\end{aligned}$$

Since we are working with a biological system, negative population densities are not allowed. Therefore, we only consider states (a, b, c) in $\mathbb{R}_+^3 = \{(a, b, c) \in \mathbb{R}^3 \mid a, b, c \geq 0\}$ (Zeeman, 1993). Fixed point \mathbf{x}_8^* does not always lie in \mathbb{R}_+^3 , while fixed points \mathbf{x}_5^* , \mathbf{x}_6^* and \mathbf{x}_7^* do. The following equalities should hold so that one of the densities at fixed point \mathbf{x}_8^* becomes zero:

$$\begin{aligned}a_8^* = 0 &\Leftrightarrow P_3 = -\frac{(P_2 - 1)(P_1 + P_2 - 1)}{P_2}, \\ b_8^* = 0 &\Leftrightarrow P_3 = \frac{1}{2} \left(2 - P_1 - P_2 \pm \sqrt{P_1^2 + 2P_1P_2 - 4P_1 + P_2^2} \right), \\ c_8^* = 0 &\Leftrightarrow P_3 = \frac{-P_1^2 - P_1P_2 + 2P_1 - 1}{P_1 - 1}.\end{aligned}\tag{3.8}$$

These three surfaces thus cut out a region in the winning probability parameter space where fixed point \mathbf{x}_8^* does not lie in \mathbb{R}_+^3 , as visualised with grey shades in Figure 3.4.

Stability of the fixed points

The next step involves studying the stability of the fixed points. When a dynamical system is at a fixed point, it can stay there for an infinite amount of time, or a perturbation can push it away from that fixed point, possibly forcing the system to end up somewhere else. A fixed point is defined to be stable if all sufficiently small perturbations away from the fixed point damp out in time, so that the system eventually returns to the original fixed point. Conversely, a fixed point is called unstable if perturbations grow over time. The stability of

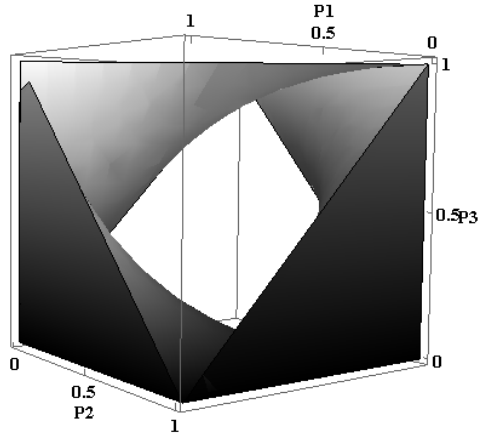


Figure 3.4: The region in the winning probability parameter space where fixed point $\mathbf{x}_8^* \notin \mathbb{R}_+^3$ is visualised with grey shades.

the fixed points can be studied through linearisation of the governing equations, using the Jacobian matrix (J) of the system (Strogatz, 1994). The elements $J_{i,j}$ of the Jacobian matrix of System (3.6) are given by:

$$\begin{aligned}
 J_{11} &= 1 - 2a^* + b^*(P_1 - 2) - c^*(P_3 + 1), \\
 J_{12} &= a^*(P_1 - 2), \\
 J_{13} &= -a^*(P_3 + 1), \\
 J_{21} &= -b^*(P_1 + 1), \\
 J_{22} &= 1 - 2b^* + c^*(P_2 - 2) - a^*(P_1 + 1), \\
 J_{23} &= b^*(P_2 - 2), \\
 J_{31} &= c^*(P_3 - 2), \\
 J_{32} &= -c^*(P_2 + 1), \\
 J_{33} &= 1 - 2c^* + a^*(P_3 - 2) - b^*(P_2 + 1).
 \end{aligned}$$

where a^* , b^* and c^* are the population densities at a fixed point.

The densities at each fixed point can now be substituted into the Jacobian, and the eigenvalues and corresponding eigenvectors of the resulting matrix can be calculated. Based on the sign of the eigenvalues, one can determine whether the directions corresponding to the eigenvectors are unstable or stable. More precisely, a positive sign corresponds to unstable behaviour, and vice versa. The fixed points for System (3.6) are classified in Table 3.1 following the rules found in Nolte (2014).

Fixed point	Eigenvalues $(\lambda_1, \lambda_2, \lambda_3)$	Classification
\mathbf{x}_1^*	$(1, 1, 1)$	Repellor
\mathbf{x}_2^*	$(-1, -P_1, -1 + P_3)$	If $\lambda_2, \lambda_3 \neq 0$: Attracting node
\mathbf{x}_3^*	$(-1, -1 + P_1, -P_2)$	If $\lambda_2, \lambda_3 \neq 0$: Attracting node
\mathbf{x}_4^*	$(-1, -1 + P_2, -P_3)$	If $\lambda_2, \lambda_3 \neq 0$: Attracting node
\mathbf{x}_5^*	$\left(\begin{array}{c} \frac{P_1(P_1-1)}{P_1(P_1-1)-1}, -1, \\ \frac{1-P_3+P_1(P_1+P_2+P_3-2)}{P_1(P_1-1)-1} \end{array} \right)$	If $\lambda_1, \lambda_3 \neq 0$: Saddle node index 1 or 2
\mathbf{x}_6^*	$\left(\begin{array}{c} \frac{P_3(P_3-1)}{P_3(P_3-1)-1}, -1, \\ \frac{1-P_2+P_3(P_1+P_2+P_3-2)}{P_3(P_3-1)-1} \end{array} \right)$	If $\lambda_1, \lambda_3 \neq 0$: Saddle node index 1 or 2
\mathbf{x}_7^*	$\left(\begin{array}{c} \frac{P_2(P_2-1)}{P_2(P_2-1)-1}, -1, \\ \frac{1-P_1+P_2(P_1+P_2+P_3-2)}{P_2(P_2-1)-1} \end{array} \right)$	If $\lambda_1, \lambda_3 \neq 0$: Saddle node index 1 or 2
\mathbf{x}_8^*	$(-1, \#, \#)$	If $\lambda_2, \lambda_3 \neq 0$: Spiral saddle index 2 or Saddle node index 2

Table 3.1: The fixed points of System (3.6) are classified using the eigenvalues of the Jacobian (Strogatz, 1994; Nolte, 2014). The eigenvalues of fixed point \mathbf{x}_8^* are too complicated to fit the table.

We now see how the introduction of the winning probabilities P_1 , P_2 and P_3 impacts the system used by Reichenbach et al. (2008). Fixed points \mathbf{x}_2^* , \mathbf{x}_3^* and \mathbf{x}_4^* are stable, and thus attract trajectories, whereas they are saddle nodes in the case of deterministic competition. Fixed points \mathbf{x}_5^* , \mathbf{x}_6^* and \mathbf{x}_7^* are saddle nodes with either one or two unstable eigendirections, called saddle node index 1 and 2, respectively (Nolte, 2014). Eigenvalue λ_1 at these three fixed points is always positive, while eigenvalue λ_3 is either negative or positive. The sign changes when P_3 takes the following values:

$$\begin{aligned}
\lambda_3(\mathbf{x}_5^*) = 0 &\Leftrightarrow P_3 = -\frac{(P_2-1)(P_1+P_2-1)}{P_2}, \\
\lambda_3(\mathbf{x}_6^*) = 0 &\Leftrightarrow P_3 = \frac{1}{2} \left(2 - P_1 - P_2 \pm \sqrt{P_1^2 + 2P_1P_2 - 4P_1 + P_2^2} \right), \\
\lambda_3(\mathbf{x}_7^*) = 0 &\Leftrightarrow P_3 = \frac{-P_1^2 - P_1P_2 + 2P_1 - 1}{P_1 - 1}.
\end{aligned} \tag{3.9}$$

These are the same equations that determine whether \mathbf{x}_8^* lies in \mathbb{R}_+^3 (Eqs. (3.8)). When the winning probabilities of the system are thus altered so that the coexistence fixed point leaves

\mathbb{R}_+^3 , then, at the same time, eigenvalue λ_3 of one of the fixed points \mathbf{x}_5^* , \mathbf{x}_6^* or \mathbf{x}_7^* will become positive, hence providing this fixed point with a second unstable eigendirection. Moreover, it can be confirmed that the regions cut out by the surfaces defined by Eqs. (3.9) only intersect when $P_1 = 0$ and $P_3 = 1$, or $P_2 = 1$ and $P_3 = 0$, or $P_1 = 2$ and $P_2 = 0$, while otherwise they are disjoint. At most one of the fixed points \mathbf{x}_5^* , \mathbf{x}_6^* and \mathbf{x}_7^* can thus be a saddle node index 2.

Eigenvalues λ_2 and λ_3 of fixed point \mathbf{x}_8^* can either be real or imaginary, and the real part of λ_3 is always strictly positive. It then follows from a proof by Zeeman (1993) that the real part of λ_2 is also positive. Therefore, when λ_2 and λ_3 are imaginary, \mathbf{x}_8^* is a spiral saddle index 2, which repels trajectories on the invariant manifold. When the eigenvalues are real, the fixed point becomes a saddle node index 2, and also repels trajectories on the invariant manifold, but not in a spiralling manner.

A proof was presented by Zeeman and van den Driessche (1998), from which it can be concluded that System (3.6) does not possess any limit cycles. Since all trajectories approach the invariant manifold, and since there are no other attractors on the invariant manifold than fixed points, we can conclude that fixed points \mathbf{x}_2^* , \mathbf{x}_3^* and \mathbf{x}_4^* are the only attractors of System (3.6) (Strogatz, 1994).

The previous findings thus show that the dynamics of System (3.6) on the invariant manifold can be divided in three classes, displayed in Figure 3.5. To obtain these figures, the dynamics on the invariant manifold were projected on the unit simplex, for which it holds that $a+b+c = 1$, so that the dynamics can be conveniently displayed (Zeeman, 1993). Figure 3.5 (a) displays the dynamics when $\mathbf{x}_8^* \in \mathbb{R}_+^3$ and two eigenvalues of \mathbf{x}_8^* have an imaginary part, (b) when $\mathbf{x}_8^* \in \mathbb{R}_+^3$ and the eigenvalues of \mathbf{x}_8^* are real, and (c) when $\mathbf{x}_8^* \notin \mathbb{R}_+^3$.

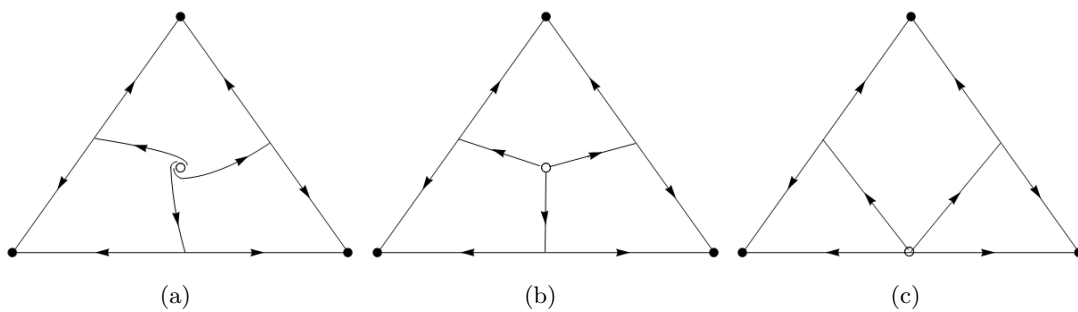


Figure 3.5: The three possible classes of dynamics of System (3.6) on the invariant manifold are displayed on the unit simplex. When a fixed point attracts on the invariant manifold, it is displayed by (\bullet), and when it repels, by (\circ). Fixed points acting as saddle nodes on the invariant manifold can be found at the intersection of their unstable and stable manifolds. The dynamics when $\mathbf{x}_8^* \in \mathbb{R}_+^3$ and two eigenvalues of \mathbf{x}_8^* have an imaginary part is displayed in (a), when $\mathbf{x}_8^* \in \mathbb{R}_+^3$ and the eigenvalues of \mathbf{x}_8^* are real in (b), and when $\mathbf{x}_8^* \notin \mathbb{R}_+^3$ in (c).

Impact of non-deterministic competition on the mean-field equations

As explained in Section 3.3.1, May and Leonard (1975) concluded that the mean-field equations without winning probabilities could produce sustained coexistence due to trajectories approaching the heteroclinic orbit while never reaching it, although this behaviour was deemed unrealistic for a real ecosystem. However, the analysis of the mean-field equations involving the winning probabilities shows that the heteroclinic connection between fixed points \mathbf{x}_2^* , \mathbf{x}_3^* and \mathbf{x}_4^* does not exist, and thus neither does the endless approach to the heteroclinic orbit. These findings are confirmed by Zeeman (1993). The mean-field equations for non-deterministic competition thus indicate that a trajectory will end up in a state where only one species survives, thus jeopardizing any possibility of sustained coexistence of the three species.

Relation between mean-field dynamics and sustained coexistence in the IBM

It can now be stated whether or not there is a relation between the three classes of dynamics shown in Figure 3.5, and the number of generations for which species managed to coexist in the IBM simulations. Therefore, Figure 2.9, where the number of generations required for a single species to become the sole survivor in the IBM was displayed as a function of the winning probabilities, has been reproduced in Figure 3.6. The regions where $\mathbf{x}_g^* \notin \mathbb{R}_+^3$ and where $\mathbf{x}_g^* \in \mathbb{R}_+^3$ while two eigenvalues of \mathbf{x}_g^* are imaginary are indicated. For the region in between, it then holds that $\mathbf{x}_g^* \in \mathbb{R}_+^3$ while all eigenvalues of \mathbf{x}_g^* are real. The figures show no clear relationship between the three classes of dynamics and the number of generations for which species managed to coexist in the IBM simulations. In Figures 3.6 (a) and (b), the region of coexistence seems to fit quite neatly in the region where \mathbf{x}_g^* has two imaginary eigenvalues. To state that this region thus predicts sustained coexistence is a mistake, however, because of the situation in Figure 3.6 (c). The region where $\mathbf{x}_g^* \notin \mathbb{R}_+^3$ seems to occur where coexistence between three species is a short term phenomenon. However, as short term coexistence also occurs outside of this region, it is not possible to predict where sustained coexistence occurs based on the three classes of dynamics.

As stated earlier, trajectories of System (3.6) are attracted to a fixed point where only one species survives. Coexistence is thus a transient phenomenon, which eventually disappears. The time it takes for a trajectory to travel from the initial condition to the vicinity of one of the attracting fixed points, \mathbf{x}_2^* , \mathbf{x}_3^* or \mathbf{x}_4^* , will therefore quantify how long species manage to coexist under the mean-field assumptions, and could possibly give an indication of how long coexistence persists in the IBM. Calculating how long a trajectory travels, however, is often impossible when working with non-linear systems. Subsequently, several measures have been devised that enable an approximation (Neubert and Caswell, 1997). Often, these measures require numerical methods, or are not adequate for the duration we want to calculate. How-

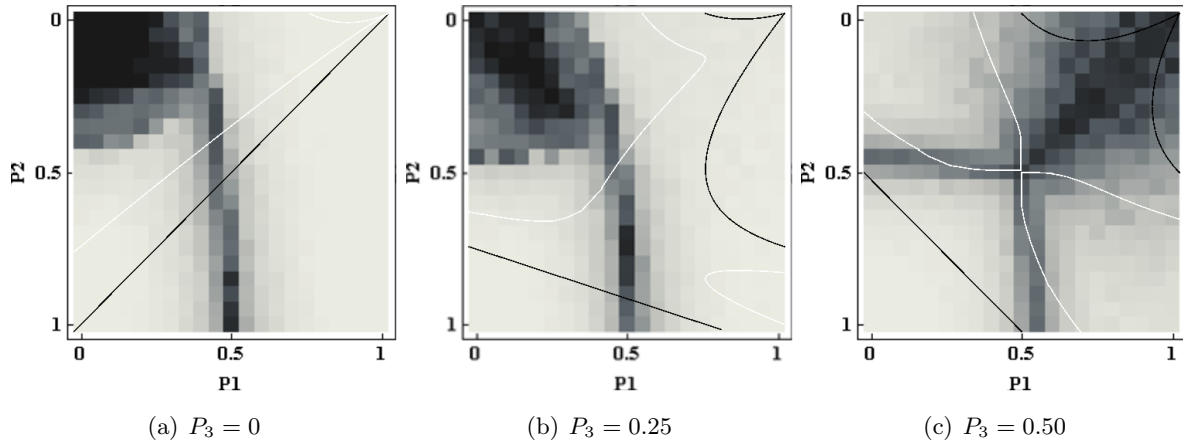


Figure 3.6: The impact of the dynamics of the coexistence fixed point on the number of generations that were required for a single species to become the sole survivor. In regions restricted by the edges of the frame and the white curves, \mathbf{x}_8^* has two imaginary eigenvalues and $\mathbf{x}_8^* \in \mathbb{R}_+^3$, while in regions restricted by the edges of the frame and the black curves, $\mathbf{x}_8^* \notin \mathbb{R}_+^3$. For the region in between, it holds that $\mathbf{x}_8^* \in \mathbb{R}_+^3$ while \mathbf{x}_8^* has three real eigenvalues.

ever, one measure that could be used is called resilience, which gives an indication of how fast perturbations to a stable state decay. It could be used to qualitatively indicate how fast a trajectory approaches \mathbf{x}_2^* , \mathbf{x}_3^* or \mathbf{x}_4^* , once it is in the vicinity of one of these fixed points (Neubert and Caswell, 1997).

The resilience of a system at a fixed point is defined as the opposite of the largest eigenvalue of the Jacobian evaluated at that fixed point. Thus high resilience corresponds to fast decay. In our case, we only considered the eigenvalues that determine the dynamics on the invariant manifold, since the other eigenvalue, determining attraction to the invariant manifold, always equals minus one. Also, since there are three attracting fixed points, we calculated the average of the resilience at each of these three fixed points. The average resilience was calculated for several sets of winning probabilities, in Figure 3.7. Comparing this figure with Figure 2.9 shows that the average resilience is high in the region of coexistence. Stating that high resilience invokes sustained coexistence, however, would be too bold. Also, the abrupt transition from sustained coexistence to short term coexistence shown in Figure 2.9 contrasts with the gradual change of the resilience through the parameter space.

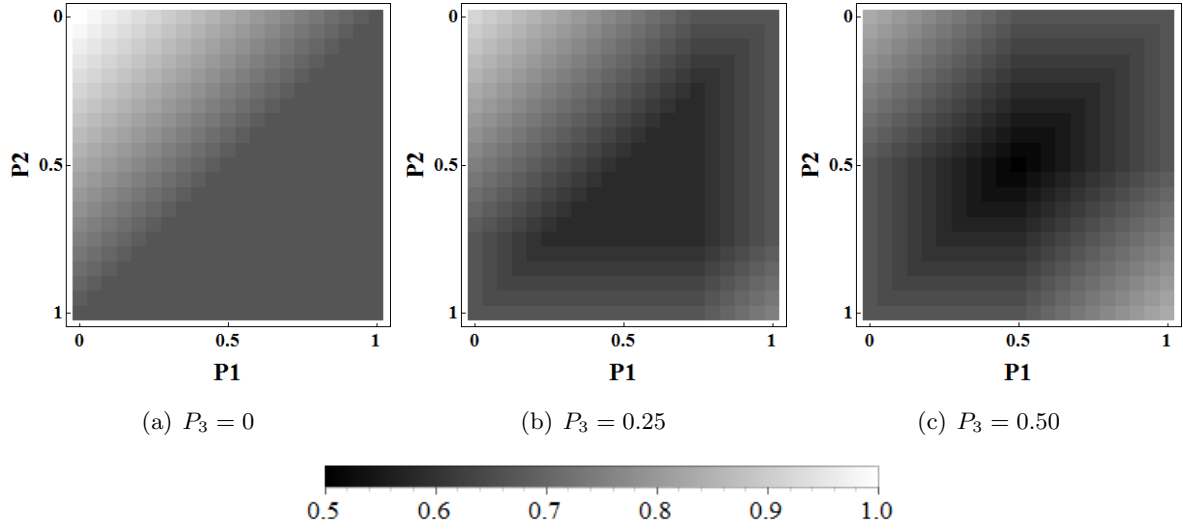


Figure 3.7: Average resilience of the attracting nodes of System (3.6).

3.4 Partial differential equations

Since neglecting space impedes the applicability of System (3.6), we will now introduce the dependence of the population densities on both time and space, and add a diffusion coefficient. In this way, the following PDEs are obtained:

$$\begin{cases} \partial a_t(\mathbf{r}, t) = D\Delta a(\mathbf{r}, t) + \mu a(\mathbf{r}, t)[1 - \rho(\mathbf{r}, t)] - \sigma P_3 a(\mathbf{r}, t)c(\mathbf{r}, t) - \sigma(1 - P_1)a(\mathbf{r}, t)b(\mathbf{r}, t) \\ \partial b_t(\mathbf{r}, t) = D\Delta b(\mathbf{r}, t) + \mu b(\mathbf{r}, t)[1 - \rho(\mathbf{r}, t)] - \sigma P_1 b(\mathbf{r}, t)a(\mathbf{r}, t) - \sigma(1 - P_2)b(\mathbf{r}, t)c(\mathbf{r}, t) \\ \partial c_t(\mathbf{r}, t) = D\Delta c(\mathbf{r}, t) + \mu c(\mathbf{r}, t)[1 - \rho(\mathbf{r}, t)] - \sigma P_2 c(\mathbf{r}, t)b(\mathbf{r}, t) - \sigma(1 - P_3)c(\mathbf{r}, t)a(\mathbf{r}, t) \end{cases} \quad (3.10)$$

with $\mathbf{r} = (r_1, \dots, r_d)$ in the d -dimensional lattice considered, D a diffusion constant and Δ the Laplacian operator.

The two-dimensional version of these equations was solved numerically using Mathematica, over the domain $[0, 1] \times [0, 1] \times [0, 1000]$. A random initial condition was used, and the winning probabilities were all set equal to one. The resulting solution, shown in Figure 3.8, displays spiral waves after a short transient. These spiral waves will exist for an infinite amount of time. When comparing the PDE solution to the spatio-temporal evolution of an IBM simulation, shown in Figure 2.5, it can be stated that the spiral waves are more clearly visible in the former. Also, when considering the plot of the densities through time, the densities of the PDE solution oscillate in a regular way, while those in the IBM simulation oscillate rather irregularly. Both these discrepancies result from the fact that the IBM simulations consider finite populations, and are thus subject to fluctuations. Still, the PDEs seem to be a more appropriate tool for gaining insight into the behaviour of the IBM than the other approaches

described in this chapter. We will analyse these further in Chapter 4, examining numerical solutions of the PDEs, and applying analytical approaches to the PDEs.

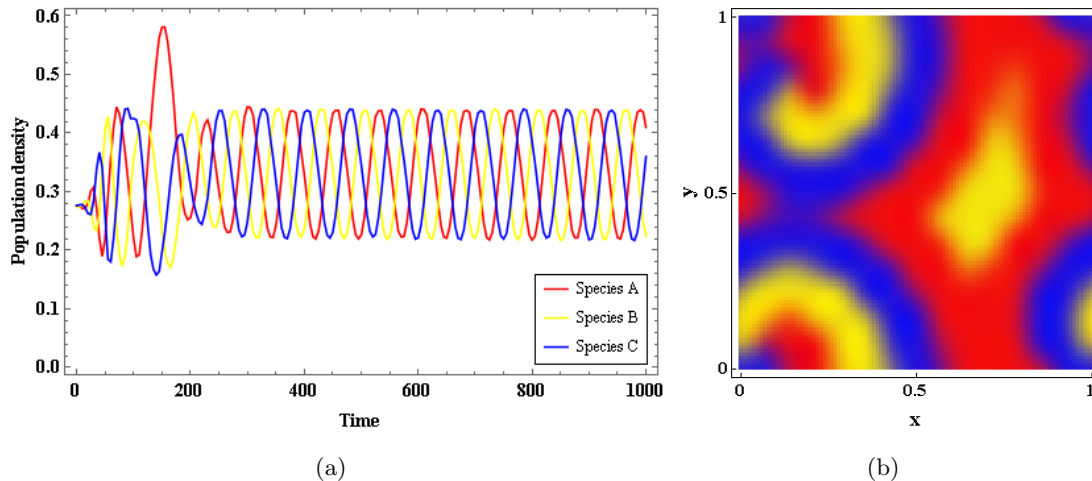


Figure 3.8: Numerical solution of the two-dimensional version of System (3.10). Figure (a) shows the evolution of the species densities through time, while Figure (b) displays the the densities in space at time $t = 1000$.

3.5 Conclusion

System (3.2), constructed in Section 3.1, seems to approximate the behaviour of the IBM simulations, without making use of stochastic interactions. Although we will not use this system of equations in this thesis, it might make for an interesting tool to investigate the IBM's dynamics.

The dynamics of the mean-field equations, just like with the IBM simulations, indicates that the introduction of winning probabilities shortens the amount of time that species can coexist. However, the results obtained in Section 3.3.2 do not adequately explain why certain combinations of winning probabilities allow species to live together for a longer time than other combinations. This could be due to the fact that space is neglected, since it has been stated that it is essential to consider the spatial distribution of species, as only then is one able to analyse the phenomena that produce sustained coexistence (Solé and Bascompte, 2006). Additionally, the difficult analysis of non-linear DEs hampers obtaining useful results.

Because of these mediocre results, we will attempt to explain sustained coexistence using PDEs. Although the analysis of PDEs is usually more complicated, they take into account the spatial distribution of the species' densities, which allows us to investigate the impact of pattern formation on coexistence.

CHAPTER 4

In-depth study of the governing partial differential equations

4.1 Three transients

In order to succeed in explaining why certain combinations of winning probabilities allow for sustained coexistence, it is essential to keep the spatial distribution of species in consideration, as only then one can study pattern formation. Of course, when one wants to use the presence and absence of spiral waves (Cfr. Section 2.3.1) in order to explain sustained coexistence, two-dimensional space should be considered. However, this often seems to be a tedious job, and has so far only led to limited success. Although Reichenbach et al. (2008) managed to obtain some characteristics of the spiral waves through recasting System (1.3) into the form of a complex Ginzburg-Landau equation, this approach seems too coarse to explain the influence of winning probabilities on coexistence.

Luckily, in one dimension, the system seems to exhibit a one-dimensional counterpart of spiral waves, called travelling waves (Rulands et al., 2011). A travelling wave is a wave with a constant shape which travels through space at a constant speed (Murray, 2002). To illustrate this, System (3.10) was solved numerically in one dimension for different winning probabilities, using Mathematica with appropriate initial and boundary conditions. All calculations were carried out using the same initial conditions, and the diffusion coefficient was set to $D = 10^{-4}$. This value corresponds to the mobility $\epsilon = 1$ used in the IBM simulations, since $D = \epsilon N^{-2}$ (Rulands et al., 2011). The equations were solved over the domain $(x, t) \in [0, 1] \times [0, 1200]$.

The species densities are plotted next to each other for several instances in time and through one-dimensional space in Figure 4.1. Figure 4.1(a) shows a travelling wave that will continue to exist for infinite time, as species A (red) chases species B (yellow) with the same speed as species B chases species C (blue) and C chases A. In Figure 4.1(b), species A chases

species B slightly slower than in Figure 4.1(a). Therefore, after some time, the travelling wave configuration will be destroyed and replaced by a more complicated and seemingly irregular pattern. These irregular waves exist for a large but finite amount of time, and seem visually similar to certain cellular automata. In Figure 4.1(c), both the travelling wave and the irregular wave are short-lived, while in Figure 4.1(d), the irregular wave does not emerge after the travelling waves are destroyed.

From these space-time diagrams, one could conclude that the progression from an initial condition to a monoculture is subject to three transients. We will define the first transient to be the transition from the initial condition to the second transient. The second transient is then the travelling wave transient, where three travelling domains, one for each species, chase each other. The third transient will be the irregular transient. The duration of these transients will determine how long coexistence persists, and will probably also give an indication of the duration of coexistence in IBM simulations.

4.2 Travelling waves

At first glance, the travelling wave transient appears to be the easiest to analyse, since its behaviour is quite straightforward. Figure 4.2(a) displays the profile of the travelling wave that was depicted in Figure 4.1(a), at time $t = 60$. If we know the wave speed of the travelling wave between two species as a function of the winning probability governing the competition between those species, we would have a good idea of how long the second transient persists. The goal of this section is thus to obtain this wave speed.

4.2.1 Lotka-Volterra equations for two species

Considering Figure 4.2(a), it is clear that at the wave front, the density of the third species is very small. It may therefore be reasonable to assume that the travelling wave between two species can be approximately described by tracking the interaction between only two species, while ignoring the dynamics of the third species. System (3.10) then reduces to

$$\begin{cases} \frac{\partial a}{\partial t}(\mathbf{r}, t) = D \Delta a(\mathbf{r}, t) + \mu a(\mathbf{r}, t) [1 - a(\mathbf{r}, t) - b(\mathbf{r}, t)] - \sigma (1 - P_1) a(\mathbf{r}, t) b(\mathbf{r}, t), \\ \frac{\partial b}{\partial t}(\mathbf{r}, t) = D \Delta b(\mathbf{r}, t) + \mu b(\mathbf{r}, t) [1 - a(\mathbf{r}, t) - b(\mathbf{r}, t)] - \sigma P_1 b(\mathbf{r}, t) a(\mathbf{r}, t). \end{cases} \quad (4.1)$$

To verify that this simplified system also has travelling wave solutions, as System (3.10), it was again solved using Mathematica, and the result is shown in Figure 4.2(b).

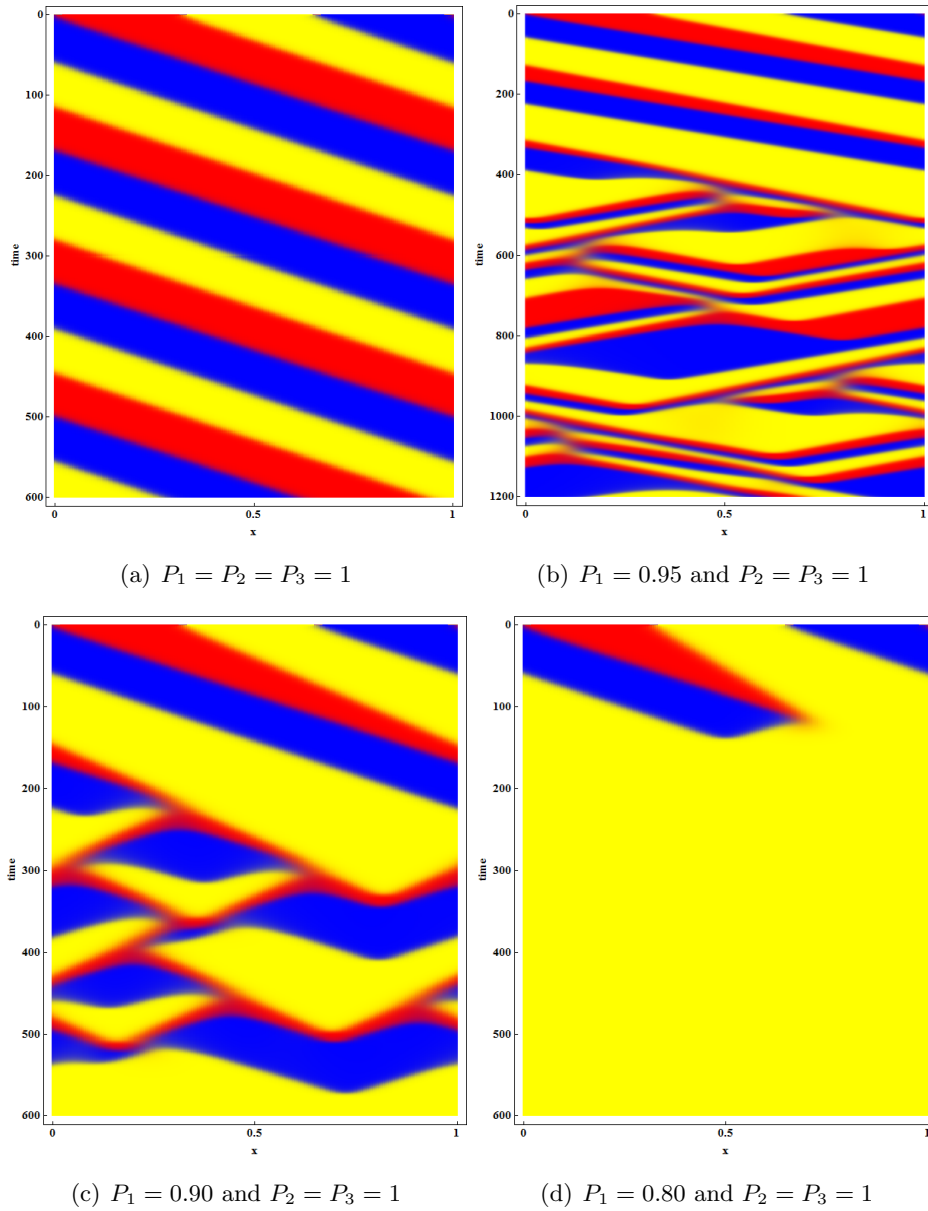


Figure 4.1: Numerical solutions of the one-dimensional counterpart of System (3.10) for different winning probabilities.

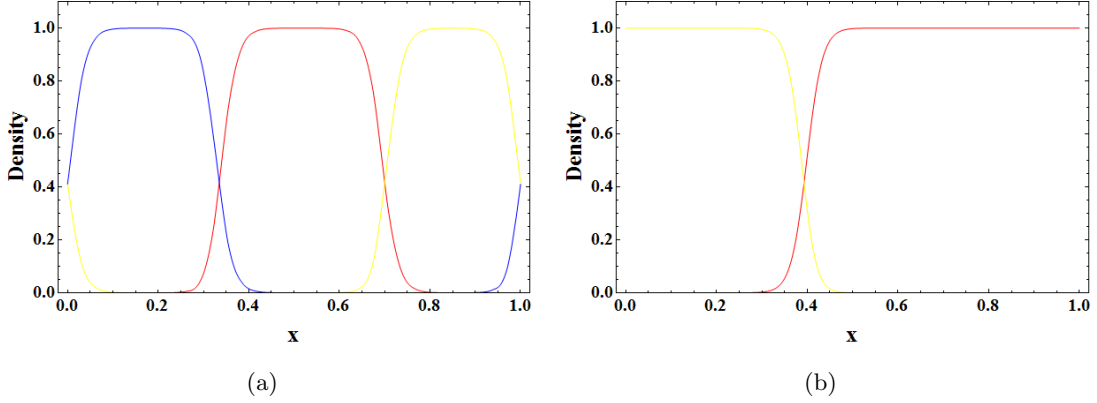


Figure 4.2: Profile of the travelling wave solution of System (3.10), as displayed on Figure 4.1(a) at time $t = 60$ (a) and a travelling wave solution of System (4.1) (b).

We can now rescale time and space by introducing $t^* = \mu t$ and $x^* = \sqrt{\mu/D}x$ and we take $k = \sigma/\mu$. For the sake of brevity, the asterisks are dropped in the remainder, we stop writing down the dependence on space and time explicitly, and denote $\frac{\partial a}{\partial t}$ by a_t and $\frac{\partial^2 a}{\partial x^2}$ by a_{xx} , so that the system becomes

$$\begin{cases} a_t = a_{xx} + a[1 - a - (1 + k(1 - P_1))b], \\ b_t = b_{xx} + b[1 - (1 + kP_1)a - b]. \end{cases} \quad (4.2)$$

Since we are interested in the impact of the winning probabilities, we will take $k = 1$.

System (4.2) is a specific case of a more general system of Lotka-Volterra equations for two species with diffusion (Hung, 2012; Lotka, 1920), given by

$$\begin{cases} a_t = a_{xx} + a[1 - a - \alpha_1 b], \\ b_t = d b_{xx} + \gamma b[1 - \alpha_2 a - b], \end{cases} \quad (4.3)$$

where d , γ , α_1 and α_2 are positive parameters. By setting $d = 1$, $\gamma = 1$, $\alpha_1 = 2 - P_1$ and $\alpha_2 = 1 + P_1$, one obtains System (4.2). As indicated in Section 3.3.2, it should hold that $a \geq 0$ and $b \geq 0$ since we are working with a biological system. Equivalently, all $(a, b) \in \mathbb{R}_+^2$.

It is known that System (4.3) has four fixed points, $\mathbf{x}_1^* = (0, 0)$, $\mathbf{x}_2^* = (1, 0)$, $\mathbf{x}_3^* = (0, 1)$ and $\mathbf{x}_4^* = (\frac{1-\alpha_1}{1-\alpha_1\alpha_2}, \frac{1-\alpha_1}{1-\alpha_1\alpha_2})$. This last one corresponds to coexistence, and does not always lie in \mathbb{R}_+^2 . The stability of the fixed points divide the dynamics into four possible regimes as a function of α_1 and α_2 (Hung, 2012):

1. $\alpha_1 < 1 < \alpha_2$: \mathbf{x}_2^* is the only stable fixed point;
2. $\alpha_2 < 1 < \alpha_1$: \mathbf{x}_3^* is the only stable fixed point;
3. $\alpha_1, \alpha_2 > 1$: \mathbf{x}_2^* and \mathbf{x}_3^* are both stable;
4. $\alpha_1, \alpha_2 < 1$: \mathbf{x}_4^* is the only stable fixed point.

System (4.2) belongs to Case Three, also called the bistable case.

4.2.2 Minimal wave speed

General system

Analysing travelling waves usually involves the coordinate transformation $z = x - ct$, with c the wave speed. By doing so, the coordinate system essentially moves at the same speed as the wave, so that it observes a stationary solution. The sign of c then determines in which direction the wave travels. Applying this transformation to System (4.3) yields:

$$\begin{cases} 0 = a'' + ca' + a[1 - a - \alpha_1 b], \\ 0 = d b'' + cb' + \gamma b[1 - \alpha_2 a - b], \end{cases} \quad (4.4)$$

where the prime is used to denote the derivative with respect to z . This system can now be converted into a four-dimensional system of first order ODEs. We do so by defining $v = a'$ and $w = b'$:

$$\begin{cases} a' = v, \\ b' = w, \\ v' = -cv - a[1 - a - \alpha_1 b], \\ dw' = -cw - \gamma b[1 - \alpha_2 a - b]. \end{cases} \quad (4.5)$$

With a travelling wave solution, the system is at a steady state for $z \rightarrow -\infty$ and for $z \rightarrow +\infty$ (Murray, 2002). When considering the travelling wave from Figure 4.2(b), for instance, we indeed notice that $(a, b)(-\infty) = (1, 0)$ and $(a, b)(+\infty) = (0, 1)$, which are both fixed points of System (4.3), and correspond to fixed points $(1, 0, 0, 0)$ and $(0, 1, 0, 0)$ of System (4.5). A travelling wave solution, in the context of the latter system, thus looks like a trajectory connecting $(1, 0, 0, 0)$ and $(0, 1, 0, 0)$ in the phase space (Murray, 2006). The path this trajectory describes in four-dimensional space can provide insight into the wave speed. In order to illustrate this, we will first consider Case One. After that, the method will be applied to Case Three, as this is where System (4.2) belongs.

Case One

Let us consider System (4.3) with $\alpha_1 < 1 < \alpha_2$, i.e. Case One. For this setting, Kan-on (1997) proved that the minimal wave speed is $c_{min} \geq 2\sqrt{1-\alpha_1}$ for a travelling wave with $(a, b)(-\infty) = (1, 0)$ and $(a, b)(+\infty) = (0, 1)$. The minimal wave speed is defined as $c_{min} = \inf\{c > 0 \mid \text{travelling wave with speed } c \text{ exists}\}$ (Guo and Wu, 2012). Lewis et al. (2002) proved that for a restricted parameter range, it holds that $c_{min} = 2\sqrt{1-\alpha_1}$. An intuitive argument for these results, although not a strict proof, can be made by assessing the stability of the involved fixed points of System (4.5).

The eigenvalues of the system linearised around fixed point $(0, 1, 0, 0)$ are $\lambda_{1,2} = -\frac{1}{2}c \pm \sqrt{c^2 + 4\gamma}$ and $\lambda_{3,4} = -\frac{1}{2}c \pm \sqrt{c^2 + 4(\alpha_1 - 1)}$. Eigenvalues $\lambda_{1,2}$ are always real, but the argument of the square root in the expression for $\lambda_{3,4}$ can be negative, causing the trajectory to spiral around the fixed point before reaching it, since the eigenvalues become imaginary. Due to this spiralling, density a becomes negative at some point, which is biologically meaningless. If we require eigenvalues $\lambda_{3,4}$ to be real, it is necessary that $c \geq 2\sqrt{1-\alpha_1}$, which is the minimal wave speed stated earlier (Murray, 2006; Okubo et al., 1989). It has been conjectured that the actual speed c of the travelling wave is equal to the minimal wave speed c_{min} (Murray, 2006). Although this often seems to be true, Hosono (1998) found a numerical example for which this is not the case. However, it is clear that finding a minimal wave speed would give us an indication of the actual wave speed.

Case Three

Let us now consider System (4.5) with $d = 1$, $\gamma = 1$, $\alpha_1 = 2 - P_1$ and $\alpha_2 = 1 + P_1$, as in System (4.2). Eigenvalues of this system linearised around $(1, 0, 0, 0)$ are $\lambda_{1,2} = -\frac{1}{2}c \pm \sqrt{c^2 + 4}$ and $\lambda_{3,4} = -\frac{1}{2}c \pm \sqrt{c^2 + 4(1 - P_1)}$, and those around $(0, 1, 0, 0)$ are $\lambda_{1,2} = -\frac{1}{2}c \pm \sqrt{c^2 + 4}$ and $\lambda_{3,4} = -\frac{1}{2}c \pm \sqrt{c^2 + 4P_1}$. Unfortunately, the eigenvalues are always real since $0 \leq P_1 \leq 1$, so that we do not have a means to find a restriction on the wave speed.

Rigorous results for the parameter ranges of Case Three are rather limited. It was proved by Gardner (1982), Conley and Gardner (1984) and Kan-on (1995), using different methods, that a travelling wave connecting $(a, b)(-\infty) = (1, 0)$ and $(a, b)(+\infty) = (0, 1)$ exists and is unique. Moreover, Kan-on (1995) proved that this solution is monotone with a wave speed c for which it holds that $-2 < c(\gamma, \alpha_1, \alpha_2) < 2\sqrt{\gamma d}$, with $c(\gamma, \alpha_1, \alpha_2)$ depending monotonically on the parameters γ , α_1 and α_2 .

The sign of the wave speed determines in which direction the wave travels. In our case, it indicates whether species A chases species B or the other way around. Guo and Lin (2013) proved that the sign of the travelling wave connecting $(a, b)(-\infty) = (1, 0)$ and $(a, b)(+\infty) = (0, 1)$ in System (4.3), with $\gamma = d$, is given by:

$$\text{sign}[c(\gamma, \alpha_1, \alpha_2, d)] = \begin{cases} 1, & \text{if } \alpha_2 > \alpha_1 > 1, \\ 0, & \text{if } \alpha_2 = \alpha_1 > 1, \\ -1, & \text{if } \alpha_1 > \alpha_2 > 1. \end{cases}$$

Applying this to System (4.2), $P_1 = 0.5$ should result in a standing wave with speed $c = 0$. Intuitively, this is indeed what one should expect, as both species are equally strong when $P_1 = 0.5$. This was confirmed by numerically solving System (4.2). When $P_1 > 0.5$, $\alpha_2 > \alpha_1$ and thus the wave travels in the direction where $(a, b) = (0, 1)$. This again tallies with the fact that when $P_1 > 0.5$, species A is stronger than species B. Similar arguments hold for $P_1 < 0.5$, and were confirmed numerically, as will be discussed in Section 4.2.4.

From all the results stated above, we cannot derive an exact or approximate wave speed $c(P_1)$ for System (4.2). Our hope is that this system is in some way simpler than the general System (4.4), so that a wave speed can be obtained.

4.2.3 Exact solutions

It is possible to obtain some analytical travelling wave solutions connecting $(a, b)(-\infty) = (1, 0)$ and $(a, b)(+\infty) = (0, 1)$ for specific values of the parameters in System (4.4) (Rodrigo and Mimura, 2001, 2000; Kudryashov, 2012; Kudryashov and Zakharchenko, 2015). Figure 4.2(b) indicates that the travelling wave solution has the form of a hyperbolic tangent. Since the derivative of this function is expressible in terms of itself, it is assumed that $\frac{da}{dz} = F(a)$. Furthermore, it is assumed that $b = G(a)$. Substituting these expressions into System (4.3), the following system is obtained:

$$\begin{cases} 0 = & F \frac{dF}{da} + cF & + & a[1 - a - \alpha_1 G], \\ 0 = d & \left(F \frac{dF}{da} \frac{dG}{da} + F^2 \frac{d^2 G}{da^2} \right) + cF \frac{dG}{da} & + \gamma & G[1 - \alpha_2 a - G]. \end{cases} \quad (4.6)$$

The forms of F and G are assumed to be $F(a) = \sum_{i=0}^m k_i a^i$ and $G(a) = \sum_{i=0}^n l_i a^i$, respectively (Rodrigo and Mimura, 2000). The boundary conditions $(a, b)(-\infty) = (1, 0)$ and $(a, b)(+\infty) = (0, 1)$ can now be imposed, and a relation between n and m can be established by substituting the general forms of F and G into System (4.6) and balancing the highest order terms of the derivatives with those of the nonlinear Lotka-Volterra terms. A value for m can now be chosen, and its counterpart n can be calculated (Rodrigo and Mimura, 2000).

Substituting these specific forms for F and G into System (4.6) results in two polynomials that are a function of a . If the coefficients accompanying the terms in a equal zero, the forms of F and G solve the system. Setting all coefficients equal to zero yields a system of equations

that can be solved for specific Lotka-Volterra parameter values, so that all coefficients k_i and l_i are obtained (Rodrigo and Mimura, 2000).

However, the solutions obtained in this way require Lotka-Volterra parameter values different from the ones in System (4.2). We are thus not able to obtain an exact solution, and an exact wave speed, using this method. A hyperbolic tangential function was fitted to the numerical solution of System (4.2), as shown in Figure 4.3. The almost immaculate fit indicates how close the solution we are seeking for is to the hyperbolic tangential form.

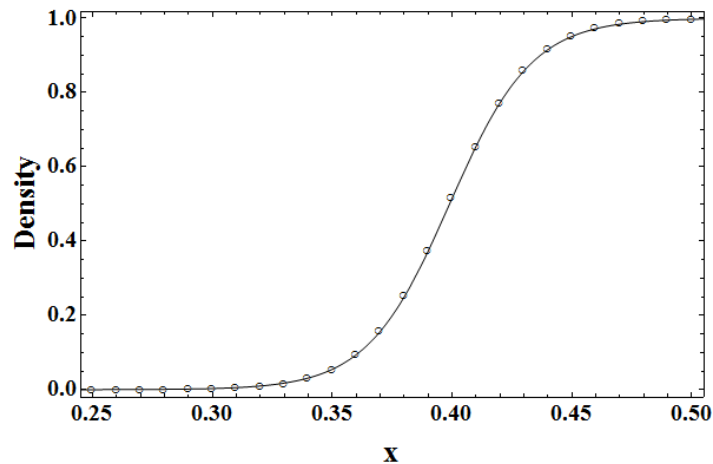


Figure 4.3: The graph of $\frac{1}{2} [1 + \tanh[a_0(z - z_0)]]$ fitted to data (\circ) from a numerical travelling wave calculation.

4.2.4 Approximating the wave speed

Let us now consider the Lotka-Volterra system for two species, without diffusion:

$$\begin{cases} \frac{da}{dt} = a[1 - a - (2 - P_1) b], \\ \frac{db}{dt} = b[1 - (1 + P_1) a - b]. \end{cases} \quad (4.7)$$

These equations were already given for three species in Section 3.3.2. The phase portrait for System (4.7), in Case Three, is shown in Figure 4.4. Fixed points $(1, 0)$ and $(0, 1)$ are stable, fixed point $(0, 0)$ is unstable and the coexistence fixed point is a saddle node. Zeeman (1993) proved that there exists an invariant manifold, also called the carrying simplex, which attracts every non-zero trajectory. All fixed points, except $(0, 0)$ thus lie on this manifold. The aim of the following section is to approximate the equation describing this manifold, and then, since the manifold attracts all non-zero trajectories, to confine the dynamics for System (4.7) to

this manifold, so that we hopefully obtain a one-dimensional DE that can approximate the behaviour of System (4.7). For this equation, we will then attempt to derive a wave speed.

Change of coordinate system

The approximation of the invariant manifold has been done for System (1.2) by Reichenbach et al. (2008). We use their method as inspiration for approximating the invariant manifold in the case of System (4.2).

The unstable manifold of the coexistence fixed point lies on the invariant manifold. The eigenvector of the system at the coexistence fixed point corresponding to a positive eigenvalue will thus be tangent to the invariant manifold. This vector, \mathbf{y}_a , is shown in Figure 4.4. Orthogonal to this vector, we construct a vector \mathbf{y}_b . We will transform the coordinate system so that the axes of the new coordinate system are aligned with \mathbf{y}_a and \mathbf{y}_b , and we will require that the coexistence fixed point becomes the new origin.

The coordinates of the coexistence fixed point are $(-\frac{1-P_1}{-1-P_1+P_1^2}, -\frac{P_1}{-1-P_1+P_1^2})$, and the system's unstable eigendirection at that point is $\mathbf{v}_1 = \mathbf{y}_a = (\frac{-2+P_1}{1+P_1}, 1)$, while the stable eigendirection is $\mathbf{v}_2 = (-1 + \frac{1}{P_1}, 1)$. We now construct a vector orthogonal to \mathbf{y}_a , i.e. $\mathbf{y}_b = (1, \frac{2-P_1}{1+P_1})$. To obtain the new coordinates $\mathbf{Y} = (Y_a, Y_b)$, we thus perform the transformation $\mathbf{Y} = S \mathbf{x}$ with $\mathbf{x} = (a + \frac{1-P_1}{-1-P_1+P_1^2}, b + \frac{P_1}{-1-P_1+P_1^2})$ and $S = \begin{pmatrix} \frac{-2+P_1}{1+P_1} & 1 \\ 1 & \frac{2-P_1}{1+P_1} \end{pmatrix}$. Expressing the old coordinates in terms of the new ones, we can use these expressions in System (4.7) to obtain a system of ODEs in terms of $d_t Y_a$ and $d_t Y_b$.

Approximating the invariant manifold

We now search for an expression of the invariant manifold $Y_b = G(Y_a)$. We choose to approximate it up to third order, and thus we take $G(Y_a) = J(P_1)Y_a + K(P_1)Y_a^2 + L(P_1)Y_a^3$, with parameters $J(P_1)$, $K(P_1)$ and $L(P_1)$ to be determined. Since trajectories stay on the invariant manifold, we know that $d_t G(Y_a) = \frac{\partial G}{\partial Y_a} d_t Y_a = d_t Y_b$. Thus, $\frac{\partial G}{\partial Y_a} d_t Y_a = (J(P_1) + 2K(P_1)Y_a + 3L(P_1)Y_a^2) d_t Y_a = d_t Y_b$. We substitute $d_t Y_b$ and $d_t Y_a$ calculated earlier into this equation, and in order to make the equation hold up to third order, we find the values for the coefficients $J(P_1)$, $K(P_1)$ and $L(P_1)$, given in Appendix B. In this way, we have now approximated the invariant manifold. Upon substituting our new expression for Y_b into the equation for $d_t Y_a$, we obtain:

$$d_t Y_a = c_0(P_1)Y_a + c_1(P_1)Y_a^2 + c_2(P_1)Y_a^3, \quad (4.8)$$

with $c_0(P_1)$, $c_1(P_1)$ and $c_2(P_1)$ given in Appendix B.

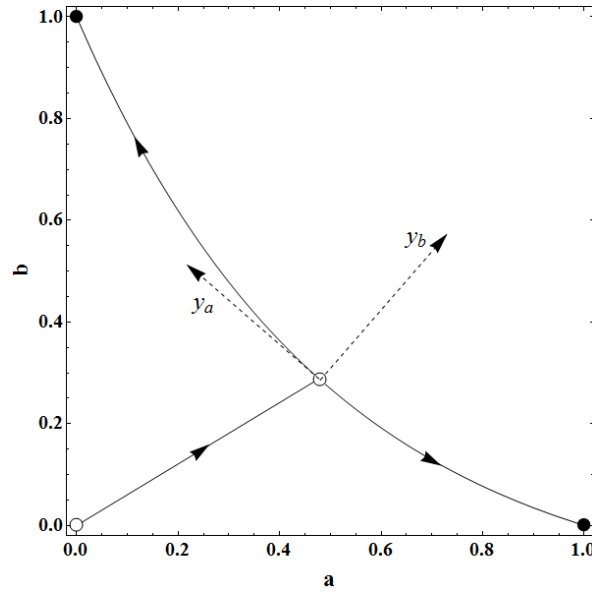


Figure 4.4: The phase plane of System (4.7) for some generic value of P_1 . Stable fixed points are represented by (●) and unstable fixed points by (○). An invariant manifold connects the coexistence fixed point with the fixed points where only one species survives. The vectors \mathbf{y}_a and \mathbf{y}_b are displayed.

This ODE has three fixed points: $Y_1(P_1) \leq 0$, $Y_2 = 0$ and $Y_3(P_1) \geq 0$. Using this, ODE (4.8) can be rewritten to obtain

$$d_t Y_a = c_2(P_1) Y_a (Y_a - Y_1(P_1)) (Y_a - Y_3(P_1)), \quad (4.9)$$

with $Y_1(P_1)$ and $Y_3(P_1)$ as in Appendix B.

It can be verified that the fixed point $Y_1(P_1)$ then corresponds to the fixed point $(1, 0)$ in System (4.7), while $Y_3(P_1)$ corresponds to $(0, 1)$. Note that the third order approximation of the invariant manifold conveniently assures that $d_t Y_a$ is equal to a polynomial of third degree, with one negative root and one positive, surrounding a root at the origin. Both the negative and the positive fixed points are stable, while the fixed point at the origin is unstable. This is indeed the behaviour we want to approximate (cfr. Figure 4.4).

Solving the approximate equation with diffusion

Now, we reintroduce diffusion in Equation (4.9) and make Y_a dependent on space again, which yields:

$$\partial_t Y_a = \partial_{xx} Y_a + c_2(P_1) Y_a (Y_a - Y_1(P_1)) (Y_a - Y_3(P_1)). \quad (4.10)$$

Again, we choose $z = x - ct$ and obtain:

$$0 = Y_a'' + cY_a' + c_2Y_a(Y_a - Y_1)(Y_a - Y_3) = L(Y_a), \quad (4.11)$$

and we look for a travelling wave solution with $Y_a(-\infty) = Y_1(P_1)$ and $Y_a(+\infty) = Y_3(P_1)$. Murray (2002) proposes an approach to solve a similar equation. The following ansatz is used:

$$Y_a' = r(Y_a - Y_1(P_1))(Y_a - Y_3(P_1)), \quad (4.12)$$

where r is a parameter, to be determined. This ODE can be solved analytically:

$$Y_a(z) = \frac{Y_3(P_1) + KY_1(P_1) \exp(r(Y_3(P_1) - Y_1(P_1))z)}{1 + K \exp(r(Y_3(P_1) - Y_1(P_1))z)}, \quad (4.13)$$

with K some constant that shifts the solution along the z -axis. This solution has some properties we want for the solution of Equation (4.11), as $Y_a(-\infty) = Y_1(P_1)$ and $Y_a(+\infty) = Y_3(P_1)$ when r is negative. If we now substitute Equation (4.12) into Equation (4.11), we obtain:

$$L(Y_a) = (Y_a - Y_1(P_1))(Y_a - Y_3(P_1))[(2r^2 + c_2(P_1))Y_a - (r^2(Y_3(P_1) + Y_1(P_1)) - cr)] = 0. \quad (4.14)$$

Since $L(Y_a)$ must equal zero, we require $2r^2 + c_2(P_1) = 0$ and $r^2(Y_3(P_1) + Y_1(P_1)) - cr = 0$. Solving this system of equations results in two solutions. We select the solution that has $r < 0$, which leads to $r(P_1) = -\sqrt{\frac{-c_2(P_1)}{2}}$ and wave speed $c(P_1) = -\sqrt{\frac{-c_2(P_1)}{2}}(Y_3(P_1) + Y_1(P_1))$. The square root of $-c_2(P_1)$ is real since it holds for $0 \leq P_1 \leq 1$ that $c_2(P_1) < 0$. If parameter $r(P_1)$ and wave speed $c(P_1)$ satisfy these restrictions, then Solution (4.13) solves Equation (4.11).

Since parameters $c_2(P_1)$, $Y_3(P_1)$ and $Y_1(P_1)$ are all functions of only P_1 , the wave speed $c(P_1)$ can be plotted as a function of P_1 , as in Figure 4.5. The approximated wave speed fits the numerically obtained wave speeds reasonably well. The error is probably due to confining the dynamics to the invariant manifold, and the approximation of this manifold up to third order only.

Travelling waves and coexistence

From the approximate travelling wave speed obtained in the previous section, we will now estimate how long the travelling wave transient exists for a certain set of winning probabilities. From an initial condition consisting of three domains, with a domain being a region in space inhabited by individuals of a single species, we will thus calculate which domain is destroyed first, and how long it takes to destroy this domain. These results will depend not only on the winning probabilities, but also on the length of the domains when the travelling wave transient emerges.

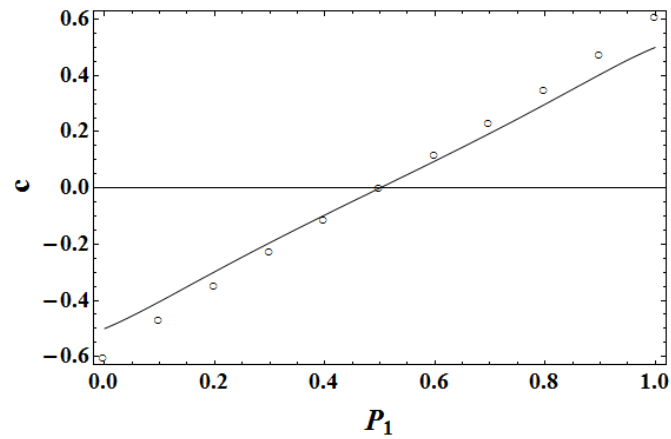


Figure 4.5: The wave speed $c(P_1) = -\sqrt{\frac{-c_2(P_1)}{2}}$ plotted against the winning probability P_1 . Wave speeds (\circ) obtained by numerically solving System (4.2) are also displayed.

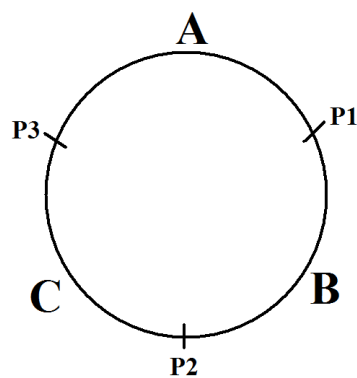


Figure 4.6: The three domains displayed on the circle, with the winning probabilities on the three wave fronts.

In Figure 4.6, the three domains are displayed on the circle, which is possible by imposing periodic boundary conditions as in the case of the IBM simulations. Competition at the wave fronts between two domains is decided by a certain winning probability. In order to calculate how fast a domain grows or shrinks, we can use the following formulae:

$$\begin{aligned}v_A &= c(P_1) - c(P_3), \\v_B &= c(P_2) - c(P_1), \\v_C &= c(P_3) - c(P_2),\end{aligned}\tag{4.15}$$

where v_A , v_B and v_C represent the growth speed of the domains belonging to species A, B and C, respectively. It can be verified that v_i is positive if the domain of i grows.

At most two domains can have a negative growth speed. For these two domains, the time until destruction t_D is given by:

$$t_{D,i} = -\frac{L_i}{v_i},\tag{4.16}$$

with v_i the growth speed and L_i the initial length of the domain concerned. The species with the smallest t_D will be the one whose domain is destroyed first, after which the travelling wave vanishes.

An extensive study can now be conducted, where for various combinations of winning probabilities and various initial domains the life span of the travelling wave transient is calculated. As this is beyond the scope of this thesis, we only consider an initial state where each domain covers 1/3 of the space, and the range of winning probabilities used for running the IBM simulations. The results of these calculations for some sets of winning probabilities are shown in Figure 4.7. In order to facilitate its comparison with Figure 2.9 ($\epsilon = 1$), winning probabilities for which an infinite amount of time is required for the first domain to be destroyed, were replaced by the maximal finite value obtained in the calculations. Also, the time was rescaled between 60 and 10 000, because these values are the minimal and maximal number of generations displayed in Figure 2.9.

When comparing Figures 4.7 and 2.9, it is clear that the travelling wave transient does not explain everything. It should be noted that the infinitely long existence of travelling waves resulting from some winning probabilities are unrealistic, as in the IBM simulation fluctuations will always destroy the travelling wave transient after some time, due to the stochastic nature of the IBM. Overall, it is clear that the first and the third transient should also be accounted for in order to properly explain where coexistence persists for a long time. Besides, it is also possible that the simplification from two dimensions to one influences the coexistence time. However, Figure 4.7 shows that it takes a significant amount of time for one domain

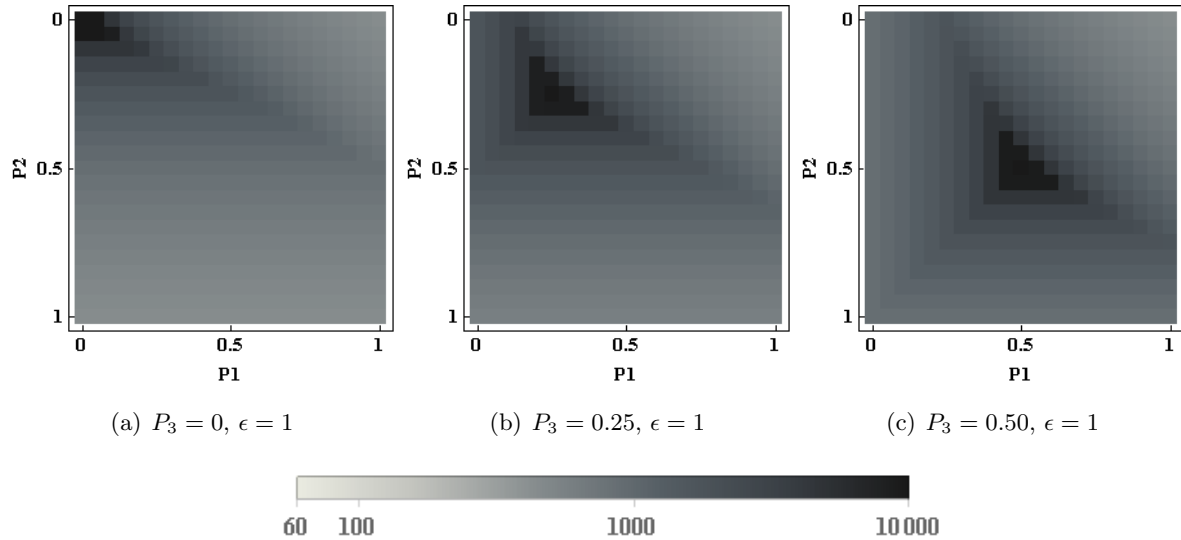


Figure 4.7: The relative time until one domain is destroyed.

to be destroyed in the region of coexistence. Thereby, it is thus confirmed that the existence of travelling waves, and their two-dimensional counterparts spiral waves, can significantly prolong the number of generations for which species manage to coexist.

4.3 Irregular waves

As indicated in Section 4.1, aside from travelling waves, solving the one-dimensional counterpart of System (3.10) can also produce irregular waves. The irregular waves observed in Figures 4.1(b) and 4.1(c) may be caused by more complex spatio-temporal dynamics than the monotone travelling waves between two species we researched in the previous section. Such dynamics include pulse waves and possibly non-monotone travelling waves (Chen et al., 2013; Ikeda, 2002, 2007). Although similar behaviour has been observed (Rulands et al., 2011; Venkat and Pleimling, 2010), it seems that no profound research has been conducted to unravel the nature of these irregularities. Although a further investigation of the irregular waves could explain an important part of the coexistence time, this is beyond the scope of this thesis. On a different note, it can be stated that this irregular behaviour holds some visual similarities to the space-time diagrams evolved by some cellular automata, such as Rule 30 (Wolfram, 1983). This becomes even more apparent for lower diffusion constants, as shown in Figure 4.8.

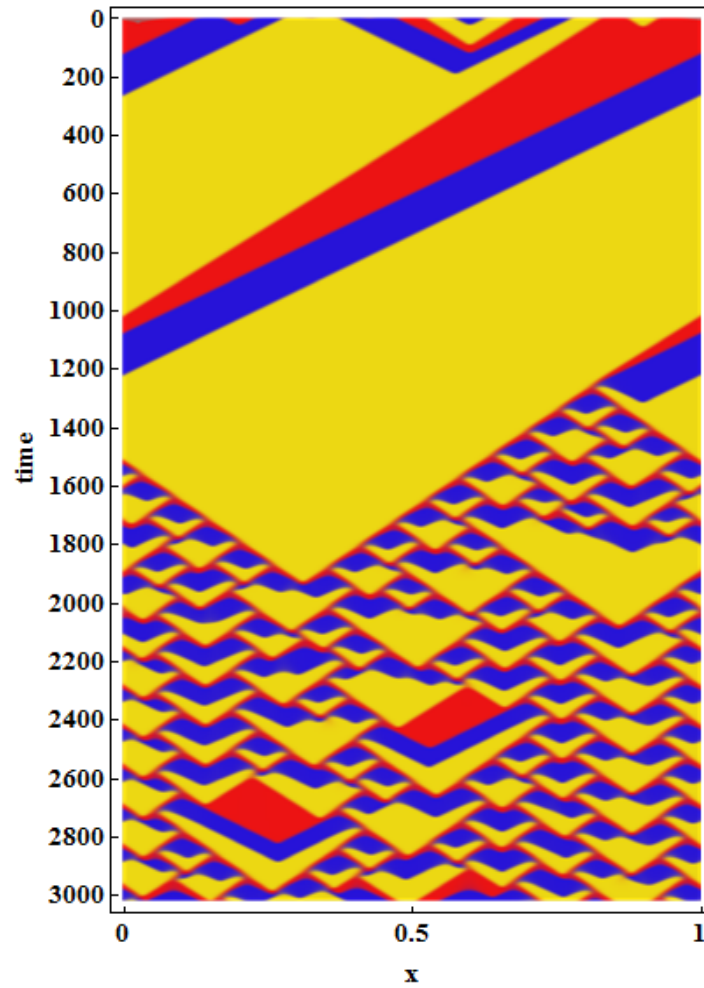


Figure 4.8: A numerical solution of System (3.10) on the domain $(x, t) \in [0, 1] \times [0, 3000]$, with $D = 3 \times 10^{-6}$.

4.4 Transient from initial condition

It is clear that the random initial configuration used in the simulations of Chapter 2 will have a strong influence on how the system behaves once it reaches the travelling wave transient. For instance, in one dimension it will partly determine the density distribution of the three species in space at the beginning of the travelling wave transient, and therefore it will also affect the lifetime of this transient.

In the IBM simulation, small domains containing only one species will emerge from the random initial conditions due to stochastic effects. This behaviour is called coarsening (Frachebourg et al., 1996; Rulands et al., 2011). These domains will then chase each other, much like travelling waves do, but on a smaller scale. Due to this small scale chasing, some domains

will vanish, while others will grow in size. At some point in time, only three domains will remain, which signifies the start of the travelling wave transient. The first transient is visible in Figure 4.8 until time 200.

Using IBM simulations, coarsening theory and the results obtained concerning travelling waves, one can research exactly how the first transient determines the densities with which the travelling wave transient starts off. This, however, is also beyond the scope of this thesis.

4.5 Conclusion

Numerical solutions of System (3.10) allowed for the identification of three transients during which coexistence persists. The duration of the second transient was investigated analytically by approximating a travelling wave speed. Although this confirmed that pattern formation can prolong coexistence significantly, the second transient does not entirely explain why sustained coexistence occurs for certain sets of winning probabilities. In order to do so, the first and third transient should also be considered. It is clear that the short first transient will strongly influence the duration of the second transient. The duration of the third transient remains an open problem, and it is also unclear how this transient will manifest itself in a two-dimensional solution of the PDEs, or in an IBM simulation. Moreover, the influence of stochasticity on the duration of the transients should be investigated in order to apply the results obtained by studying PDEs to the IBM.

CHAPTER 5

Conclusions

5.1 Conclusions

The results of the IBM simulations described in Chapter 2 show that the introduction of the winning probabilities has a disastrous impact on the duration of coexistence, as conveniently displayed in Figure 2.9. While for deterministic cyclic competition, the three species manage to maintain sustained coexistence as long as mobility is sufficiently low (Reichenbach et al., 2007), the introduction of non-deterministic competition makes this impossible for a large number of winning probability combinations (Section 2.3.3). The winning probabilities can thus play a significant role in the possibility of sustained coexistence, and it is thus important to consider them when studying coexistence.

It was also concluded that the stronger species, e.g. the species with the highest probability of beating the other two species, is often the most likely to be the sole survivor. This contradicts a study by Frean and Abraham (2001). Although this contradiction is only the result of the fact that the individuals considered in their study interact by slightly different rules than the individuals in our research, it seems appropriate to relax “survival of the weakest”, as proposed by Frean and Abraham (2001), to “survival of the least aggressive” (Section 2.4.2).

In Chapter 3 it was shown that the trajectories of the mean-field equations governing non-deterministic cyclic competition end up in a fixed point where only one species survives (Section 3.3.2). This behaviour also differs from that for deterministic cyclic competition, as trajectories in that case engage in a neverending approach towards a heteroclinic orbit, so that the three species are present at all times (May and Leonard, 1975). The dynamics of the mean-field equations thus confirms that the winning probabilities have a disastrous effect on the possibility of sustained coexistence, as species under non-deterministic competition only coexist during the transient from the initial condition to a state where one species survives.

Further investigations did not enable us to predict which combinations of winning probabilities induce sustained coexistence.

Several other modelling paradigms were considered in Chapter 3, in order to determine which one seemed the most appropriate for explaining the region of coexistence using analytical methods. A model was devised which is closely related to the IBM, but which avoids the random interactions that make the IBM stochastic. Therefore, the spatio-temporal evolution of this newly devised model is the deterministic consequence of the initial condition and the game-theoretic rules assigned to the involved individuals (Section 3.1). Although this model does not perfectly mimic the possible spatio-temporal dynamics displayed by the IBM simulation, it seems to approach it, as it exhibits phenomenological behaviour very similar to that of the IBM. It would thus be useful to investigate whether this model can be used for studying IBMs.

From the models presented in Chapter 3, the PDEs were selected for further investigation, as they account for the spatial distribution of the population densities, while, to some extent, their dynamics can be investigated in an analytical way. The PDEs were numerically solved in one-dimensional space, and, as with the mean-field equations, coexistence was only a temporary phenomenon in these solutions. The spatial distribution of the species' densities during coexistence allowed for the identification of three transients. The first transient is the transition from the initial condition to the second transient, which is characterized by travelling waves. When these travelling waves are destroyed, irregular waves emerge for some sets of winning probabilities, and this is defined as the third transient (Section 4.1). The duration of these transients determines how long species manage to coexist.

The duration of the travelling wave transient can be calculated after obtaining the three wave speeds of the wave fronts between species A and B, B and C, and C and A. However, the determination of these wave speeds, to the best of our knowledge, remains an open problem. Still, we were able to approximate them in Section 4.2.4, from which we could subsequently calculate the duration of the travelling wave transient. Although this duration partly explains why sustained coexistence occurs for certain sets of winning probabilities, it is clear that the first and third transients should also be considered (Section 4.2.4). By doing so, one could quantify the time for which species coexist in the solutions of the one-dimensional PDE, and this information could be used to explain the region of coexistence that was identified on the basis of the IBM simulations. This, however, is beyond the scope of this thesis.

5.2 Limitations

Non-deterministic cyclic competition is a broad subject. For instance, one could focus on IBM simulations and numerical solutions of the PDEs. By solving the PDEs numerically for a multitude of well-devised initial conditions, the dynamics of the three transients (Section 4.1) could be extensively researched in function of the winning probabilities. The use of IBM simulations could then indicate how these dynamics are altered by the stochastic interactions. This approach could lead to a more complete description of the emergent phenomena and their influence on the lifetime of coexistence, possibly resulting in a thesis covering an in-depth study of a well delimited, specific subject. In order to gain knowledge about non-deterministic competition in a structured way, one could start off with a simple system, and add complexity gradually. At first, a one-dimensional system without reproduction (Section 2.4.2) could be considered, or even without mobility, after which complexity could be added in order to end up with the two-dimensional one considered in our IBM simulations (Section 2.2).

Instead, a more superficial overview of the dynamics of the IBM and PDEs is presented in this thesis. By doing so, there was time to investigate specific topics which seemed particularly interesting. Although results were often not optimal, the search was always interesting and enriching.

5.3 Extensions

As stated in the previous section, an in-depth investigation of the three transients using numerical solutions of PDEs and IBM simulations is necessary. In this way, the behaviour of these transients could be aptly described as a function of the winning probabilities. The insights obtained in this way might open up possibilities for analytical approaches, to obtain a thorough understanding of the *in silico* ecosystem's dynamics.

In literature, investigating the dynamics of an IBM usually involves the construction of a PDE mimicking its behaviour. Similar to what was described in this thesis, the dynamics of the PDE is then investigated and related to the behaviour of the IBM. Although this approach can be very powerful, its frequent use could be due to the absence of a well-established theory on IBM's dynamics. However, it must be possible to properly explain why spatial patterns emerge from an IBM using only the game rules by which the individuals play. By doing so, one could quantify the relative stability (or instability) of the states and patterns emerging from an IBM. Comparing the stability of the states could provide valuable information on how they are formed and destroyed, or for how long they can exist, without having to resort to PDEs. Possibly, this theory could result from combining the theory of dynamical systems with statistical mechanics.

Finally, although it is likely that non-deterministic competition occurs in real life, this should be confirmed by conducting tests with real-world ecosystems. Moreover, a realistic range of winning probabilities should be established, to see whether they will strongly influence coexistence, or rather will be positioned in the region of coexistence.

Bibliography

- Allesina, S. and Levine, J. M. (2011). A competitive network theory of species diversity. *Proceedings of the National Academy of Sciences*, 108:5638–5642.
- Atmanspacher, H., Filk, T., and Scheingraber, H. (2005). Stability analysis of coupled map lattices at locally unstable fixed points. *The European Physical Journal B*, 44:229–240.
- Bondy, A. and Murty, U. S. R. (2008). *Graph Theory*. Graduate Texts in Mathematics. Springer, New York, United States of America.
- Brauer, F. and Castillo-Chávez, C. (2001). *Mathematical Models in Population Biology and Epidemiology*. Texts in Applied Mathematics. Springer, New York, United States of America.
- Chen, C.-C., Hung, L.-C., Mimura, M., Tohma, M., and Ueyama, D. (2013). Semi-exact equilibrium solutions for three-species competition-diffusion systems. *Hiroshima Mathematical Journal*, 43:179–206.
- Cheng, H., Yao, N., Huang, Z., Park, J., Do, Y., and Lai, Y. (2014). Mesoscopic interactions and species coexistence in evolutionary game dynamics of cyclic competitions. *Scientific Reports*, 4:10.1038/srep07486.
- Conley, C. and Gardner, R. (1984). An application of the generalized Morse index to travelling wave solutions of a competitive reaction-diffusion model. *Indiana University Mathematics Journal*, 33:319–343.
- Czárán, T. L., Hoekstra, R. F., and Pagie, L. (2002). Chemical warfare between microbes promotes biodiversity. *Proceedings of the National Academy of Sciences of the United States of America*, 99:786–790.
- De Baets, B. (2013). *Wiskunde 3: differentiaalvergelijkingen*. UGent, Ghent, Belgium.
- Ebenman, B. and Jonsson, T. (2005). Using community viability analysis to identify fragile systems and keystone species. *Trends in Ecology and Evolution*, 20:568–575.

- Ferrer, J., Prats, C., and López, D. (2008). Individual-based modelling: an essential tool for microbiology. *Journal of Biological Physics*, 34:19–37.
- Frachebourg, L., Krapivsky, P. L., and Ben-Naim, E. (1996). Spatial organization in cyclic Lotka-Volterra systems. *Physical Review E*, 54:6186–6200.
- Frean, M. and Abraham, E. R. (2001). Rock-scissors-paper and the survival of the weakest. *Proceedings of the Royal Society of London. Series B: Biological Sciences*, 268:1323–1327.
- Gardner, R. A. (1982). Existence and stability of travelling wave solutions of competition models: A degree theoretic approach. *Journal of Differential Equations*, 44:343–364.
- Gillespie, D. T. (1977). Exact stochastic simulation of coupled chemical reactions. *The Journal of Physical Chemistry*, 81:2340–2361.
- Gore, J., Youk, H., and Van Oudenaarden, A. (2009). Snowdrift game dynamics and facultative cheating in yeast. *Nature*, 459:253–256.
- Guo, J.-S. and Lin, Y.-C. (2013). The sign of the wave speed for the Lotka-Volterra competition-diffusion system. *Communications on Pure and Applied Analysis*, 12:2083–2090.
- Guo, J.-S. and Wu, C.-H. (2012). Recent developments on wave propagation in 2-species competition systems. *Discrete and Continuous Dynamical Systems - Series B*, 17:2713–2724.
- Hardin, G. (1960). The competitive exclusion principle. *Science*, 131:1292–1297.
- Hastings, A. (1997). *Population Biology: Concepts and Models*. Springer, Davis, United States of America.
- Hosono, Y. (1998). The minimal speed of traveling fronts for a diffusive Lotka-Volterra competition model. *Bulletin of Mathematical Biology*, 60:435–448.
- Huisman, J., Johansson, A. M., Folmer, E. O., and Weissing, F. J. (2001). Towards a solution of the plankton paradox: the importance of physiology and life history. *Ecology Letters*, 4:408–411.
- Huisman, J. and Weissing, F. J. (1999). Biodiversity of plankton by species oscillations and chaos. *Nature*, 402:407–410.
- Hung, L.-C. (2012). Exact traveling wave solutions for diffusive Lotka-Volterra systems of two competing species. *Japan Journal of Industrial and Applied Mathematics*, 29:237–251.

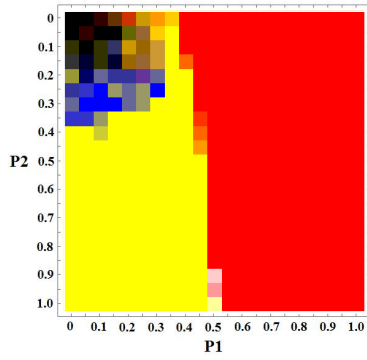
- Ikeda, H. (2002). Global bifurcation phenomena of standing pulse solutions for three-component systems with competition and diffusion. *Hiroshima Mathematical Journal*, 32:87–124.
- Ikeda, H. (2007). Dynamics of weakly interacting front and back waves in three-component systems. *Toyama Mathematical Journal*, 30:1–34.
- Jovanovic, B. and Rosenthal, R. W. (1988). Anonymous sequential games. *Journal of Mathematical Economics*, 17:77–87.
- Kan-on, Y. (1995). Parameter dependence of propagation speed of travelling waves for competition-diffusion equations. *SIAM Journal on Mathematical Analysis*, 26:340–363.
- Kan-on, Y. (1997). Fisher wave fronts for the Lotka-Volterra competition model with diffusion. *Nonlinear Analysis: Theory, Methods and Applications*, 28:145–164.
- Kaneko, K. (1993). *Theory and Applications of Coupled Map Lattices*. John Wiley & Son Ltd, Chichester, United Kingdom.
- Kerr, B., Riley, M., Feldman, M. W., and Bohannan, B. J. M. (2002). Local dispersal promotes biodiversity in a real-life game of rock-paper-scissors. *Nature*, 418:171–174.
- Kudryashov, N. A. (2012). One method for finding exact solutions of nonlinear differential equations. *Communications in Nonlinear Science and Numerical Simulation*, 17:2248–2253.
- Kudryashov, N. A. and Zakharchenko, A. S. (2015). Analytical properties and exact solutions of the Lotka-Volterra competition system. *Applied Mathematics and Computation*, 254:219–228.
- Laird, R. A. (2014). Population interaction structure and the coexistence of bacterial strains playing ‘rock-paper-scissors’. *Oikos*, 123:472–480.
- Laird, R. A. and Schamp, B. S. (2008). Does local competition increase the coexistence of species in intransitive networks? *Ecology*, 89:237–247.
- Lewis, M. A., Li, B., and Weinberger, H. F. (2002). Spreading speed and linear determinacy for two-species competition models. *Journal of Mathematical Biology*, 45:219–233.
- Liard, R. A. and Schamp, B. S. (2006). Competitive intransitivity promotes species coexistence. *The American Naturalist*, 168:182–193.
- Lotka, A. J. (1920). Analytical note on certain rhythmic relations in organic systems. *Proceedings of the National Academy of Sciences of the United States of America*, 6:410–415.
- Lutz, A. F., Risau-Gusman, S., and Arenzon, J. J. (2013). Intransitivity and coexistence in four species cyclic games. *Journal of Theoretical Biology*, 317:286–292.

- May, M. M. (1976). Simple mathematical models with very complicated dynamics. *Nature*, 261:459–467.
- May, R. M. and Leonard, W. J. (1975). Nonlinear aspects of competition between three species. *SIAM Journal on Applied Mathematics*, 29:243–253.
- Meyer-Ortmanns, H. and Thurner, S. (2011). *Principles of Evolution: From the Planck Epoch to Complex Multicellular Life*. The Frontiers Collection. Springer, Heidelberg, Germany.
- Murray, J. (2002). *Mathematical Biology I: An Introduction*. Interdisciplinary Applied Mathematics. Springer, New York, United States of America.
- Murray, J. (2006). *Mathematical Biology II: Spatial Models and Biomedical Applications*. Interdisciplinary Applied Mathematics. Springer, New York, United States of America.
- Neubert, M. G. and Caswell, H. (1997). Alternatives to resilience for measuring the responses of ecological systems to perturbations. *Ecology*, 78:653–665.
- Nolte, D. (2014). *Introduction to Modern Dynamics: Chaos, Networks, Space and Time*. Oxford University Press, Oxford, United Kingdom.
- Okubo, A., Maini, P. K., Williamson, M. H., and Murray, J. D. (1989). On the spatial spread of the grey squirrel in Britain. *Proceedings of the Royal Society of London B: Biological Sciences*, 238:113–125.
- Reichenbach, T., Mobilia, M., and Frey, E. (2006). Coexistence versus extinction in the stochastic cyclic Lotka-Volterra model. *Physical Review E*, 74.
- Reichenbach, T., Mobilia, M., and Frey, E. (2007). Mobility promotes and jeopardizes biodiversity in rock-paper-scissors games. *Nature*, 448:1046–1049.
- Reichenbach, T., Mobilia, M., and Frey, E. (2008). Self-organization of mobile populations in cyclic competition. *Journal of Theoretical Biology*, 254:368–383.
- Rodrigo, M. and Mimura, M. (2000). Exact solutions of a competition-diffusion system. *Hiroshima Mathematical Journal*, 30:257–270.
- Rodrigo, M. and Mimura, M. (2001). Exact solutions of reaction-diffusion systems and nonlinear wave equations. *Japan Journal of Industrial and Applied Mathematics*, 18:657–696.
- Rulands, S., Reichenbach, T., and Frey, E. (2011). Threefold way to extinction in populations of cyclically competing species. *Journal of Statistical Mechanics - Theory and Experiment*.
- Schreiber, S. J. and Killingback, T. P. (2013). Spatial heterogeneity promotes coexistence of rock-paper-scissors metacommunities. *Theoretical Population Biology*, 86:1–11.

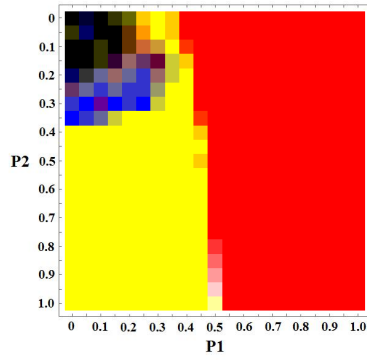
- Sherratt, T. N., Lambin, X., Petty, S. J., MacKinnon, J. L., Coles, C. F., and Thomas, C. J. (2000). Use of coupled oscillator models to understand synchrony and travelling waves in populations of the field vole *Microtus agrestis* in Northern England. *Journal on Applied Ecology*, 37:148–158.
- Solé, R. and Bascompte, J. (2006). *Self-Organization in Complex Ecosystems*. Monographs in Population Biology. Princeton University Press, Princeton, United States of America.
- Strogatz, S. (1994). *Nonlinear Dynamics and Chaos: With Applications to Physics, Biology, Chemistry, and Engineering*. Advanced book program. Westview Press, Cambridge, United States of America.
- Tucker, A. W. (1980). On jargon: the prisoner’s dilemma. *Undergraduate Mathematics and Its Applications*, 1.
- Venkat, S. and Pleimling, M. (2010). Mobility and asymmetry effects in one-dimensional rock-paper-scissors games. *Physical Review E*, 81.
- Verhulst, P. F. (1838). Notice sur la loi que la population poursuit dans son accroissement. *Correspondance Mathématique et Physique*, 10:113–121.
- Von Neumann, J. and Burks, A. (1966). *Theory of Self-reproducing Automata*. University of Illinois Press, Urbana, United States of America.
- Weiss, P. (1907). L’ hypothèse du chap moléculaire et la propriété ferromagnétique. *Journal de Physique Théorique et Appliquée*, 6.
- Wolfram, S. (1983). Statistical mechanics of cellular automata. *Reviews of Modern Physics*, 55:601–644.
- Zeeman, M. L. (1993). Hopf bifurcations in competitive three-dimensional Lotka-Volterra systems. *Dynamics and Stability of Systems*, 8:189–216.
- Zeeman, M. L. and van den Driessche, P. (1998). Three-dimensional competitive Lotka-Volterra systems with no periodic orbits. *SIAM Journal on Applied Mathematics*, 58:227–234.

APPENDIX A

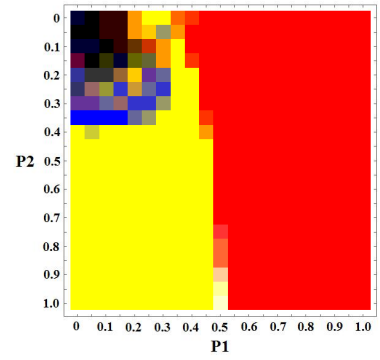
End-state parameter space at critical
mobility



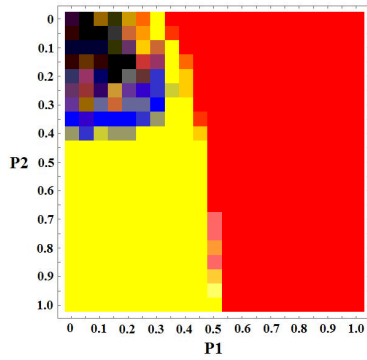
(a) $P_3 = 0$



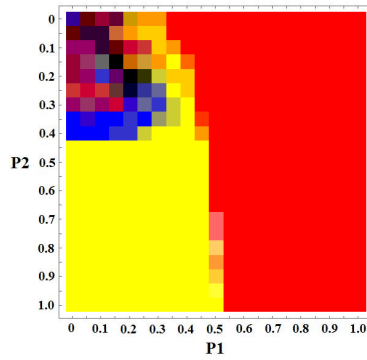
(b) $P_3 = 0.05$



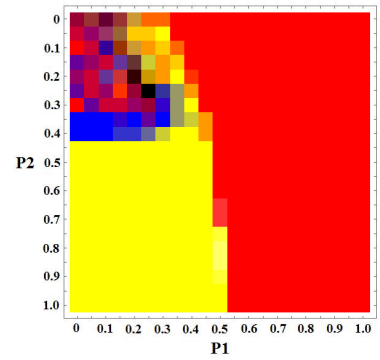
(c) $P_3 = 0.10$



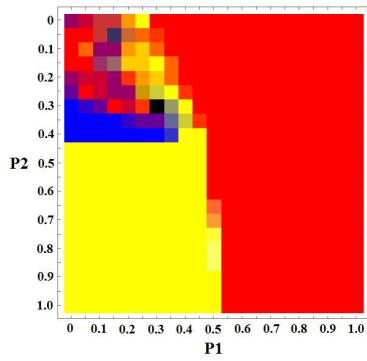
(d) $P_3 = 0.15$



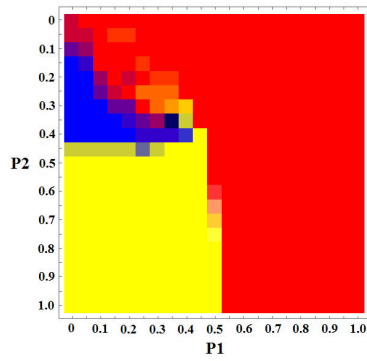
(e) $P_3 = 0.20$



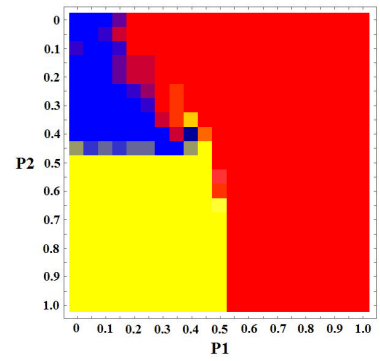
(f) $P_3 = 0.25$



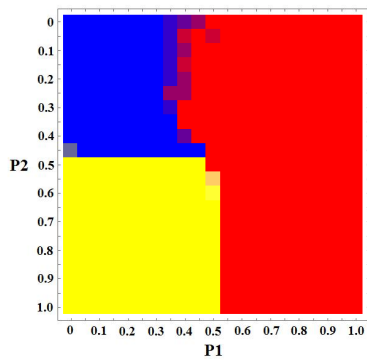
(g) $P_3 = 0.30$



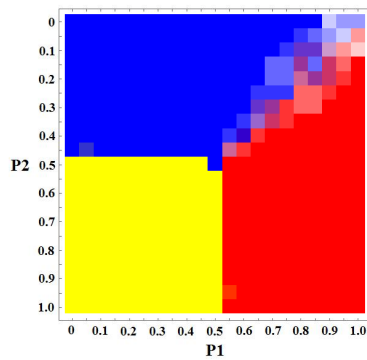
(h) $P_3 = 0.35$



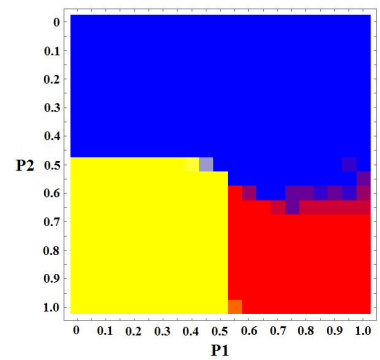
(i) $P_3 = 0.40$



(j) $P_3 = 0.45$



(k) $P_3 = 0.50$



(l) $P_3 = 0.55$

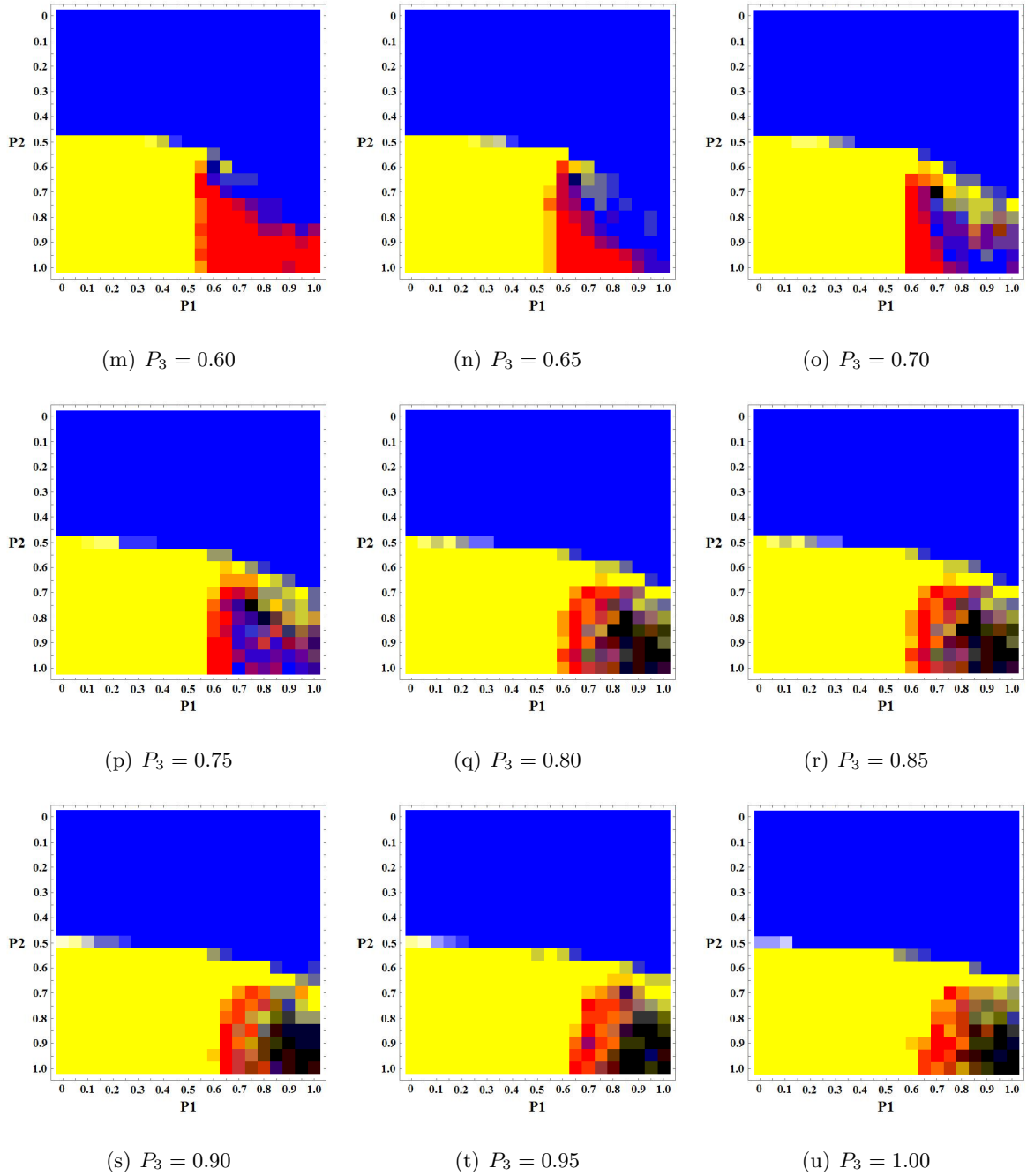


Figure A.1: The end-state parameter space resulting from the IBM simulations with $\epsilon = 2.25$, and thus at critical mobility. Black represents the region of coexistence, red represents survival of species A, blue survival of species B and yellow survival of species C, and this state was determined after 10 000 generations. P_3 increases in increments of 0.05 for every new image. P_1 and P_2 vary between zero and one on the x- and y-axis, respectively.

APPENDIX B

Coefficients in Section 4.2.4

$$J(P_1) = 0,$$

$$K(P_1) = \frac{(P_1 + 1)^2 (2P_1^5 - 8P_1^4 + 7P_1^3 + 5P_1^2 - 5P_1 - 2)}{(2P_1^2 - 2P_1 + 5)^2 (3P_1^2 - 3P_1 - 1)},$$

$$L(P_1) = \frac{2(1 + P_1)^3 (-1 - 3P_1 + P_1^2 + 4P_1^3 - 2P_1^4)^2 (2 - 19P_1 + 51P_1^2 - 49P_1^3 + 14P_1^4)}{(1 + 3P_1 - 3P_1^2)^2 (5 - 2P_1 + 2P_1^2)^4 (-1 - 4P_1 + 4P_1^2)},$$

$$c_0(P_1) = \frac{(P_1 - 1)P_1}{P_1^2 - P_1 - 1},$$

$$c_1(P_1) = -\frac{5 + 4P_1 - 36P_1^2 + 15P_1^3 + 10P_1^4 - 24P_1^5 + 16P_1^6}{(5 - 2P_1 + 2P_1^2)^2 (-1 - 3P_1 + 3P_1^2)},$$

$$c_2(P_1) = -\frac{w_0}{w_1},$$

with

$$w_0 = (1 + P_1)^3 (-1 - P_1 + P_1^2)$$

$$(50 + 237P_1 + 63P_1^2 - 1017P_1^3 + 396P_1^4 + 2184P_1^5 - 4332P_1^6 + 3804P_1^7 - 1632P_1^8 + 272P_1^9),$$

$$w_1 = (1 + 3P_1 - 3P_1^2)^2 (5 - 2P_1 + 2P_1^2)^4 (-1 - 4P_1 + 4P_1^2),$$

$$Y_1(P_1) = \frac{z_0}{z_3} (z_1 + \sqrt{z_2}),$$

$$Y_3(P_1) = \frac{z_0}{z_3} (z_1 - \sqrt{z_2}),$$

with

$$z_0 = - (2P_1^2 - 2P_1 + 5)^2 (3P_1^2 - 3P_1 - 1),$$

$$z_1 = 64P_1^7 - 224P_1^6 + 344P_1^5 - 300P_1^4 + 86P_1^3 + 59P_1^2 - 19P_1,$$

$$z_2 = 8448P_1^{14} - 59136P_1^{13} + 175744P_1^{12} - 285696P_1^{11} + 266896P_1^{10} - 125008P_1^9 \\ - 80P_1^8 + 23840P_1^7 - 640P_1^6 - 832P_1^5 - 5387P_1^4 - 58P_1^3 + 1519P_1^2 + 390P_1 + 25,$$

$$z_3 = 2(P_1 + 1)^2 (P_1^2 - P_1 - 1)$$

$$(272P_1^9 - 1632P_1^8 + 3804P_1^7 - 4332P_1^6 + 2184P_1^5 + 396P_1^4 - 1017P_1^3 + 63P_1^2 + 237P_1 + 50).$$